Athens Institute for Education and Research
ATINER

ATINER's Conference Paper Series
MEC2019-2707

Design of a New Generation Supersonic Transport Aircraft

ChaKaria Hunter
Master of Science Student
San Jose State University
USA

Nikos Mourtos
Professor and Chair
San Jose State University
USA

An Introduction to ATINER's Conference Paper Series

Conference papers are research/policy papers written and presented by academics at one of ATINER's academic events. ATINER's association started to publish this conference paper series in 2012. All published conference papers go through an initial peer review aiming at disseminating and improving the ideas expressed in each work. Authors welcome comments.

Dr. Gregory T. Papanikos
President
Athens Institute for Education and Research

This paper should be cited as follows:

Hunter, C. and Mourtos, N. (2020). **"Design of a New Generation Supersonic Transport Aircraft",** Athens: ATINER'S Conference Paper Series, No: **MEC2019-2707.**

Athens Institute for Education and Research
8 Valaoritou Street, Kolonaki, 10671 Athens, Greece
Tel: + 30 210 3634210 Fax: + 30 210 3634209 Email: info@atiner.gr URL: www.atiner.gr
URL Conference Papers Series: www.atiner.gr/papers.htm

ISSN: 2241-2891
16/04/2020

Design of a New Generation Supersonic Transport Aircraft

ChaKaria Hunter
Nikos Mourtos

Abstract

This paper presents the preliminary design of a new generation, 150-passenger, Mach 3, supersonic transport aircraft. A higher cruise Mach is chosen (Mach 3, compared to Mach 2 for the Concorde and the Tupolev 144) to ensure a more efficient cruise, as the drag coefficient peaks at Mach 1 and drops at supersonic speeds. The results show that the proposed payload and cruise speed can be met with a takeoff weight of 352,000 lbs (159,665 kg), while providing a range of 4,534 n.mi (8,397 km). Currently FAA and ICAO still restrict supersonic flights over land due to the disturbance caused by sonic boom. Although maintenance and safety issues played a role, these flight restrictions, along with the high operating cost associated with supersonic flight, were the main reasons for the retirement of the only two available supersonic transport aircraft. This project proposes a new supersonic transport aircraft design with a low boom, which will solve both problems at the same time. Firstly, a low boom design will reduce the environmental impact of the aircraft, allowing thus operations over land. This will increase airline flexibility, while planning supersonic routes around the world. Secondly, a low boom design will reduce drag, reducing thus a major component of the operating cost of the aircraft, most of which comes from the cost of the fuel. In addition to reducing the environmental impact, the proposed design is intended to make a supersonic transport more profitable for airlines.

Keywords: Supersonic, Transport, Low Boom, Design, Aircraft.

Introduction

A major focus of current aerospace research is reducing the sonic boom to acceptable levels. Supersonic travel is now possible from a manufacturing standpoint but is restricted due to the disturbances that the sonic boom causes. According to Samuel Hammond of the Niskanen Center, seven in-depth marketing analysis indicate that there is a large demand for SSTs. Of those market studies, two were conducted by Gulfstream Aerospace. It is stated that smaller business jets would be in more demand initially until airlines learn which routes are more popular for supersonic travel and only then would they invest in full size passenger jets (Hammond, 2017). Given the focus of aerospace research currently, it is obvious that organizations like NASA and Boeing are working to prove that supersonic travel over land doesn't have to be a disruption and therefore doesn't have to be restricted by the FAA (Sun & Smith, 2017).

Literature Review

Fuselage Design

The main consideration in designing the fuselage of an aircraft is reducing the many forms of drag: friction, profile, base, compressibility, and induced. Friction drag is directly related to the wetted area which is directly related to the fineness ratio. Supersonic aircrafts are designed to have high fineness ratios, which implies a relatively high drag coefficient. Compressibility drag comes from the formation of shocks on the fuselage. To minimize compressibility drag, the area rule is used. The area rule states that if the total cross-sectional area approaches a smooth distribution called the Sears-Haack body, the compressibility drag would be minimized (Roskam, 1997, 2000, 2002).

Most supersonic aircraft have a high leading-edge sweep angle, slender fuselage design that approaches the blended wing body design (BWB) due to its increased aerodynamic performance. The BWB reduces wetted area which in turn reduces the friction drag. The lift distribution is improved by the smooth incorporation of the increased lift profile of the fuselage. Because the fuselage has a high lift capability in this configuration, the wing loading is reduced. While the BWB has numerous aerodynamic advantages, there are also a few critical stability disadvantages. The pressure distribution in the blended wing body configuration is not ideal for maintaining trim and the required static stability margin. Many shape optimization tools have been developed to determine a balance between maintaining the aerodynamic advantages and reducing the stability disadvantages through methods of moving the CG position, increasing the span, reducing the sweep, and more (Lyu & Martins, 2014).

Wing Design

The wing shape of a supersonic aircraft can be a limiting factor to the amount of lift generated. Important parameters include leading edge sweep, thickness, and airfoil shape (Roskam, 2002). A study was conducted at the NASA Langley Unitary Plan Wind Tunnel to determine the effects of leading-edge sweep and airfoil shape on the flow over the wing. The leading-edge vortex flow over the wing of a supersonic aircraft generates the additional lift needed for supersonic flight and therefore need not be disturbed or reduced by geometric factors. It was determined that the airfoil shape, more than the leading edge sweep, had a greater impact on the surface flow and pressure distribution over the wing (Wood & M., 1988; Wood, Byrd, & Wesselmann, 1992).

Engine Location

The placement of the engine on an aircraft can affect weight, drag, and the efficiency of its inlet. On subsonic aircraft, the jet turbine engines are usually found mounted beneath the wings. Supersonic aircraft tend to only have the inlets mounted above or below the wing. In the paper written by Charles Trefny, the case is made to place the inlets above the wing in order to minimize the propagation of shock waves toward the ground. Through the supersonic wind tunnel testing done at NASA Glenn Research Center, it was determined that performance of the inlet, in terms of mass capture, pressure recovery, and flow distortion, demonstrates an acceptable propulsion system integration in supersonic flight although there were found to be angle of attack restrictions (Trefny, Hirt, Anderson, Fink, & Magee, 2014). NASA Langley also took on the task to evaluate the performance of the above-wing inlet on a supersonic aircraft. This investigation, though, was conducted at transonic speeds to simulate the takeoff and landing flight conditions. It was determined that effects of the jet operation at transonic speeds are negligible in terms of flow over the wing and pressure distributions (Mercer & Carson, 1979).

Tail Arrangements

The purpose of the tail is to provide control, increased stability, and trim while not increasing the drag or weight significantly. The horizontal stabilizer contributes to the longitudinal stability by producing a restoring pitching moment. The horizontal stabilizer also usually contains the elevator that allows control of the pitch of the aircraft by the pilot. The vertical stabilizer contributes to the lateral stability by creating a restoring yaw moment. This stabilizer also contains the rudder so that yaw can be controlled by the pilot. There are many possible configurations for these surfaces depending on the mission specifications of the aircraft. Many supersonic aircraft tend to combine

these surfaces in some form in order to reduce drag and weight. (Roskam, 2002)

A design by Richard Lugg employs the V-Tail in order to provide the appropriate control surfaces as well as a stabilizing and lifting surface (US20150108269A1, 2013). A design by Supersonic Aerospace International LLC uses an inverted V-Tail. The shape of the shock wave that creates the sonic boom is due to how the pressure propagates along the length of the aircraft. Common sonic boom reduction techniques create a smooth pressure distribution by creating a compression shock at the nose and an expansion shock at the tail. The Supersonic Aerospace International patent is using the inverted V-Tail to create that expansion wave at the tail to reduce the sonic boom (US006824092B1, 2003).

Low Boom Design

In many of the previous sections, methods for designing a low boom aircraft are discussed in parts. Often the solution is not as simple as implementing all the suggested solutions at once, but rather a delicate balance to maintain an aerodynamic advantage and still reduce drag and weight. The solution to this often comes in the form of optimization software that works to achieve certain design parameters while allowing other parameters to be compromised (Li & Rallabhandi, 2014).

Comparative Study of Similar Aircraft

Concorde

The Concorde (Figure 1) was designed with a low wing for several reasons. During low speed take off, the Concorde is at a very high angle of attack, higher than that of most transport aircrafts. To refrain from the tail being caught in the wake of the wings, the wings need to be lower. The low wing configuration also offers the greatest fuselage volume for passengers. Another advantage likely considered by the low wing configuration is that the landing gear can be attached directly within the wings. This approach was applied in the Concorde configuration. The drastic sweep back of the delta wing reduced drag and provided significant vorticial lift for takeoff and landing. The Concorde featured a single vertical tail. The engines were placed under the wing likely to avoid the distorted flow of the vortices on top of the wing caused by the swept delta wing (“CONCORDE SST,” 2003). Wind tunnel testing was required to ensure the boundary layer of the wing would not adversely affect engine intake efficiency. This aircraft also had a drooped nose configuration which allowed the pilots better landing visibility (“CONCORDE SST,” 2003).

Figure 1. *Concorde*

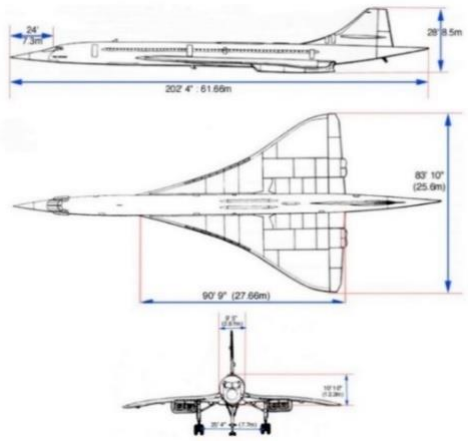

Source: Concorde SST Website.

Tupelov Tu-144

The Tu-144 (Figure 2) was designed very similar to the Concorde. It has a low, swept, delta wing configuration. This prevents deep stall at high angles of attack during takeoff and landing. It allows fuselage volume for passengers as well as allowing the landing gear to be attached directly to the wing. The sweep of the wing decreases drag but in this case did not provide quite enough lift during takeoff and so retractable canards were configured to increase lift at low speeds. The delta wing has inherent lateral stability, so a single vertical tail is configured. The engines were placed under the wings likely to allow the upper wing surface to generate as much lift as possible ("TU-144 SST," 2003). This aircraft had distinctive retractable canards as well as a breaking parachute. These two things put it far behind the Concorde in desirability by airliners. This design also featured a far more distinct drooped nose ("TU-144 SST," 2003).

Figure 2. *Tupelov Tu-144*

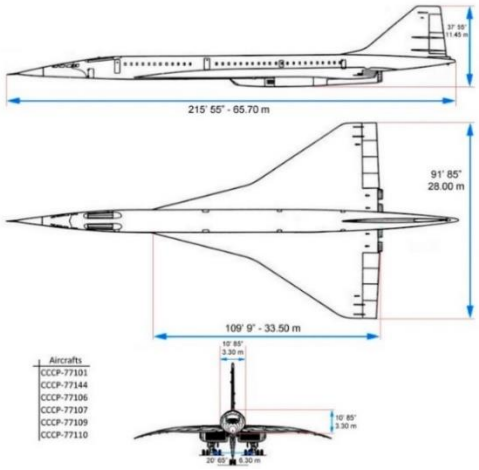

Source: Tu-144 SST Website.

Sonic Star

The SonicStar (Figure 3) is currently a conceptual design by HyperMach. This implies that changes are still being made, only comments on it as is within the patent are referenced. The conceptual design features a low wing configuration likely to allow maximized space in the fuselage for passengers. Another important consideration for having a low wing is to have the ability to place the engines on top of it without significantly increasing drag. In this position, it is believed that the engines would not disturb the lift generated by the wing because the inlets are at the most rear point of the Sears-Haack body. Due to this shape, the engines are very nearly touching at the centerline of the plane. The design also features a V-tail. It is believed that the reason for using a V-tail is to reduce the number of control surfaces and therefore reduce drag. Two of the control surfaces (rudders and elevators) are combined into a ruddervator in the V-tail design (US20150108269A1, 2013).

Figure 3. *SonicStar Configuration*

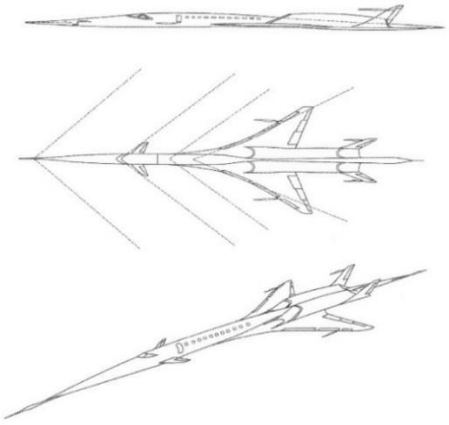

Source: SonicStar Patent Document.

Boom Co. XB-1

The Boom XB-1 (Figure 4) is also currently in the design/manufacturing process. This aircraft design features a low, delta wing to allow maximized fuselage space, increase lift and lateral stability, and to house the landing gear. It features a single vertical tail. This design has three engines likely to accommodate its range and speed specifications. There is one engine below each wing in order to not interrupt flow over the wing. There is also one engine on top of the rear fuselage, below the tail likely to decrease wing interference at the inlet (“Boom Technology SST (XB-1) Supersonic Transport Passenger Airliner - United States,” 2019).

Figure 4. *Boom Co. XB-1 Configuration*

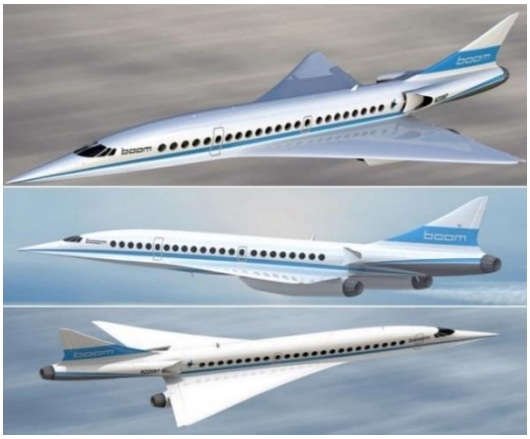

Source: Boom Company Website.

NASA X-Plane

The NASA X-Plane (Figure 5) has very little public information available. It is seen to have a wing that starts in the mid fuselage vertical location and transitions to a low wing aft of the pilot. Along with all of the previously discussed advantages of a low wing, this vertical transition allows for a much lower takeoff and landing angle of attack. The aircraft only holds the pilot as its payload and is not designed for long ranges as it is a research aircraft, therefore it only requires one engine which has been placed midline of the rear fuselage under the tail. There are also rear horizontal stabilizers below the vertical tail that are believed to decrease the sonic boom (Brake, 2016).

Figure 5. *NASA X-Plane Configuration*

Source: NASA X-Plane Website.

Methodology

The preliminary design process is outlined in detail in Dr. Jan Roskam's Aircraft Design Series and is complimented by the Advanced Aircraft Design (AAA) software. The following steps from this series are used to complete the preliminary design of this aircraft:

1. **Literature Review, Mission Specifications, and Configuration Selection**: A literature review will be conducted in order to complete a comparative study of similar aircraft and subsequently derive the mission specifications.
2. **Weight Sizing and Weight Sensitivities**: Mission weights will be calculated based on that of similar aircraft and confirmed by the AAA Program. Trade studies will be conducted on critical parameters to increase performance based on the weight sensitivities.
3. **Performance Constraints**: Constraints such as stall speed, takeoff and landing distance, and climb constraints will be calculated and compared based on FAR 25 requirements. Wing size and thrust required will be found based on those parameters.
4. **Wing Design**: The wing of the aircraft will be designed as well as any lateral control surfaces.
5. **Empennage Design**: The tail of the aircraft will be designed. The longitudinal and directional controls will also be designed in this section.
6. **Landing Gear Design**: This section calls for a preliminary calculation of the center of gravity of the aircraft.
7. **Longitudinal and Directional Stability**: Based on weight and balance calculations, the static stability of the aircraft will be determined and the aircraft will be redesigned as necessary.
8. **Drag Polar Estimation**: Zero lift drag, area ruling, and the drag polar will be calculated and addressed in this section.

Weight Sizing & Weight Sensitivities

The purpose of this section is to determine the design point of the aircraft weights using a database of similar aircraft. Determining mission weights allows us to calculate the fuel fraction necessary for the intended specifications. To analyze the effectiveness of trading one design requirement for another, weight sensitivities are found and used to conduct trade studies between critical parameters.

Mission Weight Estimates

Database for Takeoff Weights and Empty Weights of Similar Airplanes

Table 1. *Mission Weight Database*

Aircraft	**Weight Data**
Concorde("CONCORDE SST," 2003)	$W_E = 173{,}500\ lbs$ $W_{TO} = 408{,}000\ lbs$
Tupolev Tu-144("TU-144 SST," 2003)	$W_E = 202{,}400\ lbs$ $W_{TO} = 429{,}900\ lbs$
Bell X-1(Miller, 2001)	$W_E = 7{,}000\ lbs$ $W_{TO} = 12{,}250\ lbs$
Boeing X-32(Frawley, 2000)	$W_E = 22{,}490\ lbs$ $W_{TO} = 38{,}000\ lbs$
Lockheed A-12("A-12 Utility Flight Manual," 1965)	$W_E = 54{,}670\ lbs$ $W_{TO} = 117{,}000\ lbs$
Douglas D-558-2 Skyrocket(Francillon, 1988)	$W_E = 9{,}421\ lbs$ $W_{TO} = 15{,}266\ lbs$
Convair B-58(Loftin, n.d.)	$W_E = 55{,}560\ lbs$ $W_{TO} = 176{,}890\ lbs$
Douglas X-3 Stiletto(Francillon, 1988)	$W_E = 14{,}345\ lbs$ $W_{TO} = 22{,}400\ lbs$
Lockheed SR-71 Blackbird(Pace, 2004)	$W_E = 67{,}500\ lbs$ $W_{TO} = 172{,}000\ lbs$
Lockheed F-22 Raptor	$W_E = 43{,}340\ lbs$ $W_{TO} = 83{,}500\ lbs$

Determination of Regression Coefficients A and B

A log-log plot (Figure 6) was created based on the mission weight database in the previous section. Regression Coefficients A and B were determined from the plot. The values determined are comparable to those provided by Roskam's supersonic aircraft table (Roskam, 2003). These values will be used to calculate the take-off weight in the next section.

Figure 6. *Log-Log Weight Trend Plot*

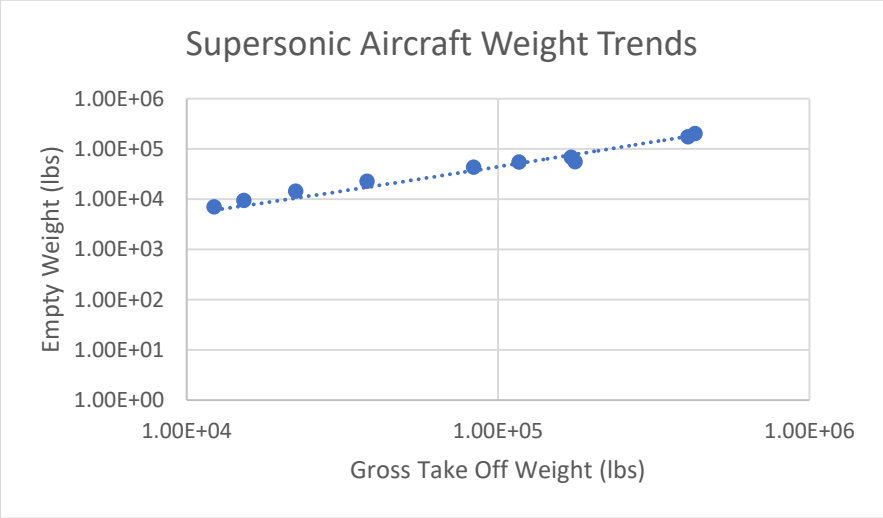

Table 2. *Regression Coefficients Comparison*

Info	A	B
Roskam's Regression Coefficients (Roskam, 2003)	0.4221	0.9897
Regression Coefficients from the above Database	0.4355	0.979

Determination of Mission Weights

Manual Calculation of Mission Weights

Weight Estimates: $W_{PL} = 41{,}000\ lbs$, $W_{crew} = 1{,}230\ lbs$, $W_{TO} = 408{,}000\ lbs$ ("CONCORDE SST," 2003). The picture of mission profile is shown in Figure 7.

Figure 7. *Mission Profile*

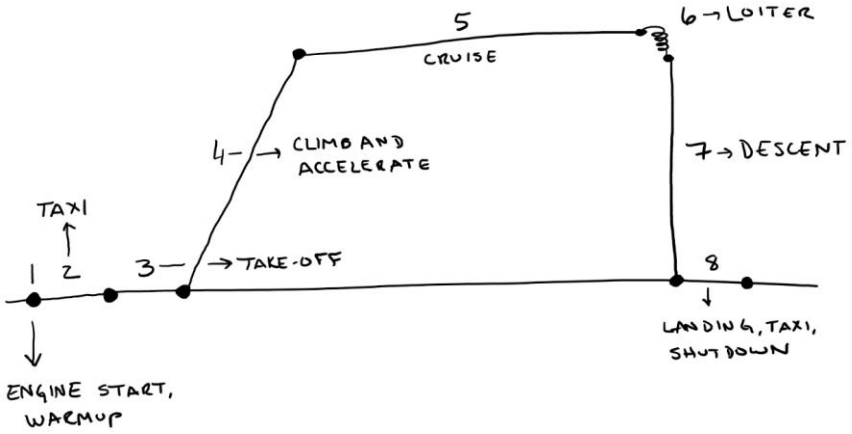

Phase 1: Engine Start and Warm Up

$$W_i = W_{TO} = 408{,}000\ lbs$$
$$W_f = W_1 = 0.990 W_{TO} = 403{,}920\ lbs$$

Phase 2: Taxi

$$W_i = W_1 = 403{,}920\ lbs$$
$$W_f = W_2 = 0.995 W_1 = 401{,}900.4\ lbs$$

Phase 3: Take-off

$$W_i = W_2 = 401{,}900.4\ lbs$$
$$W_f = W_3 = 0.995 W_2 = 399{,}890.898\ lbs$$

Phase 4: Climb to cruise altitude and accelerate to cruise speed

$$W_i = W_3 = 399{,}890.898\ lbs$$
$$W_f = W_4 = 0.89 W_3 = 355{,}902.899\ lbs$$

Phase 5: Cruise

$$W_i = W_4 = 355{,}902.899\ lbs$$
$$W_f = W_5 = {W_4}\Big/{e^{\frac{R}{\left(\frac{V}{c_j}\right)\left(\frac{L}{D}\right)}}}\quad from\ Breguet's\ Range\ Equation$$

$where\ R = 3{,}910\ NM, V = 1{,}720.7\ knots,\ {L}/{D} = 8, and\ c_j =$ 1.1 $by\ the\ design\ of\ the\ Concorde$. (“CONCORDE SST,” 2003)

$$W_f = W_5 = 260{,}398.31\ lbs$$

Phase 6: Loiter

$$W_i = W_5 = 260{,}398.31\ lbs$$

$$W_f = W_6 = {W_5}\Big/{e^{\frac{E}{\left(\frac{1}{c_j}\right)\left(\frac{L}{D}\right)}}}\quad from\ Breguet's\ Endurance\ Equation$$

$where\ E = 1\ hr, {L}/{D} = 11, and\ c_j =$ 0.7 $by\ the\ design\ of\ the\ Concorde$. (“CONCORDE SST,” 2003)

$$W_f = W_6 = 244{,}343.75\ lbs$$

Phase 7: Descent

$$W_i = W_6 = 244{,}343.75\ lbs$$
$$W_f = W_7 = 0.985 W_6 = 240{,}678.6\ lbs$$

Phase 8: Landing, Taxi, Shutdown

$$W_i = W_7 = 240{,}678.6\ lbs$$
$$W_f = W_8 = 0.992 W_7 = 238{,}753.17\ lbs$$

Mission Fuel Fraction

$$M_{ff} = \frac{W_8 W_7 W_6 W_5 W_4 W_3 W_2 W_1}{W_7 W_6 W_5 W_4 W_3 W_2 W_1 W_{TO}} = 0.5852$$
$$W_F = (1 - 0.5852) W_{TO} = 169{,}246.83\ lbs$$
$$W_{OE} = W_{TO} - W_F - W_{PL} = 197{,}753.17\ lbs$$
$$W_E = W_{OE} - 0.005 W_{TO} - W_{crew} = 194{,}483.17\ lbs$$

Allowable Value for $W_E = 178.456.4\ lbs$
$based\ on\ Regression\ Coefficients\ from\ Figure\ 6.$
Iterations of this work show that $W_{TO} = 352{,}000\ lbs$, $W_E = 162{,}000.4\ lbs$, and $W_F = 146{,}009.6\ lbs$.

Takeoff Weight Sensitivities

Manual Calculation of Takeoff Weight Sensitivities

Based on the following values, weight sensitivities were calculated.

$$W_{TO} = 352{,}000\ lbs$$
$$W_E = 162{,}000\ lbs$$
$$W_F = 146{,}009.6\ lbs$$
$$W_{PL} = 41{,}000\ lbs$$
$$W_{crew} = 1{,}230\ lbs$$
$$M_{tfo} = 0.005$$
$$M_{res} = 0\ (included\ in\ M_{ff})$$
$$M_{ff} = 0.5852$$
$$A = 0.4355\ (from\ log - \log plot)$$
$$B = 0.979\ (from\ log - \log plot)$$

For Range cases: $R = 3910\ NM,\ V = 1{,}720.7\ kts,\ \frac{L}{D} = 8,\ c_j = 1.1$ (by the design of the Concorde).

For Loiter cases: $E = 1\ hr,\ \frac{L}{D} = 11,\ c_j = 0.7$

Calculating Coefficients C, D, F

$$C = \left(1 - (1 + M_{res})\left(1 - M_{ff}\right) - M_{tfo}\right) = 0.5802$$

$$D = W_{PL} + W_{crew} = 42{,}230$$

$$F = -BW_{TO}^2(CW_{TO}(1 - B) - D)^{-1}M_{ff} = 1{,}870{,}947.983$$

Growth Factors:

Payload: $\frac{\partial W_{TO}}{\partial W_{PL}} = BW_{TO}(D - C(1 - B)W_{TO})^{-1} = 9.08\ lbs$

Empty Weight: $\frac{\partial W_{TO}}{\partial W_E} = BW_{TO}\left[invlog\left(\frac{logW_{TO} - A}{B}\right)\right]^{-1} = 2.07\ lbs$

Range: $\frac{\partial W_{TO}}{\partial R} = Fc_j\left(\frac{VL}{D}\right)^{-1} = 149.5\ lbs/NM$

Endurance: $\frac{\partial W_{TO}}{\partial E} = Fc_j\left(\frac{L}{D}\right)^{-1} = 119{,}060.33\ lbs/hr$

Cruise Speed: $\frac{\partial W_{TO}}{\partial V} = -FRc_j\left(\frac{V^2L}{D}\right)^{-1} = -339.73\ lbs/kt$

For Cruise:

Specific Fuel Consumption: $\frac{\partial W_{TO}}{\partial c_j} = FR\left(\frac{VL}{D}\right)^{-1} = 531{,}426.64\ lbs/lbs/lbs/hr$

L/D Ratio: $\frac{\partial W_{TO}}{\partial(\frac{L}{D})} = FRc_j\left(V\left(\frac{L}{D}\right)^2\right)^{-1} = -73{,}071.16\ lbs$

For Loiter:

Specific Fuel Consumption: $\frac{\partial W_{TO}}{\partial c_j} = FE\left(\frac{L}{D}\right)^{-1} = 170{,}068.18\ lbs/lbs/lbs/hr$

L/D Ratio: $\frac{\partial W_{TO}}{\partial(\frac{L}{D})} = FEc_j\left(\frac{L}{D}\right)^{-2} = -10{,}823.67\ lbs$

Trade Studies

Method

Trade studies were conducted for payload weight and range as well as specific fuel consumption and lift to drag ratio. In the first study either range or payload was increased and decreased by 10-50% of the original value. Using the sensitivity values calculated, the equivalent weight gained or loss from the takeoff weight was determined. From there, the equivalent weight that the second parameter could be changed by is found. Each of the new weights are plotted on the graphs below. In the second trade study, either specific fuel consumption or lift to drag ratio was increased or decreased by 10-50% of the original value and the previous calculations were performed.

Figure 8. *Payload vs. Range Trade Study*

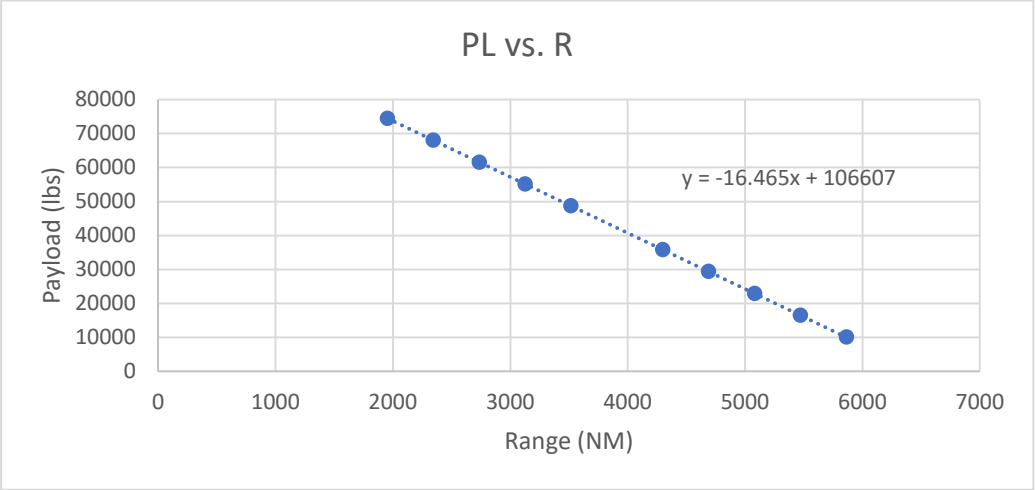

Figure 9. *Range vs. Payload Trade Study*

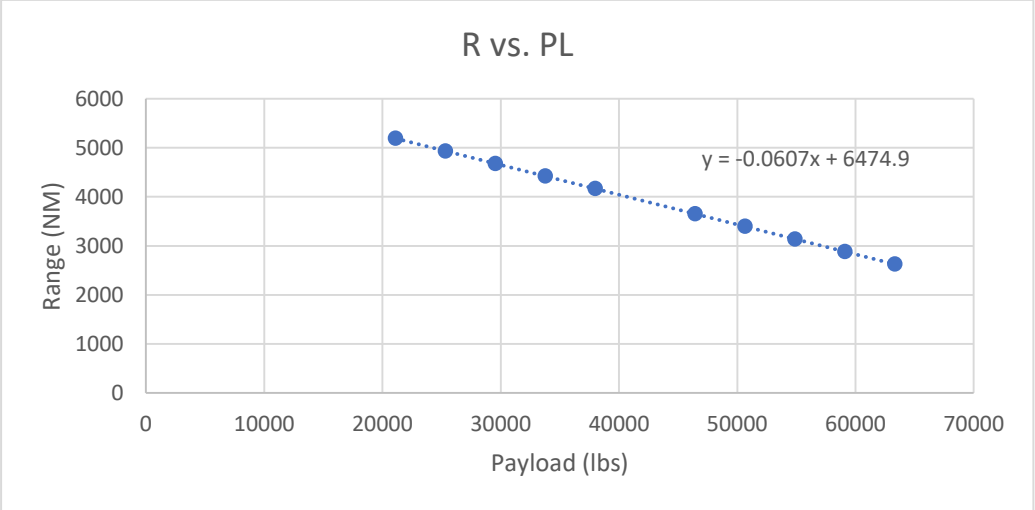

Figure 10. *L/D vs. SFC Trade Study*

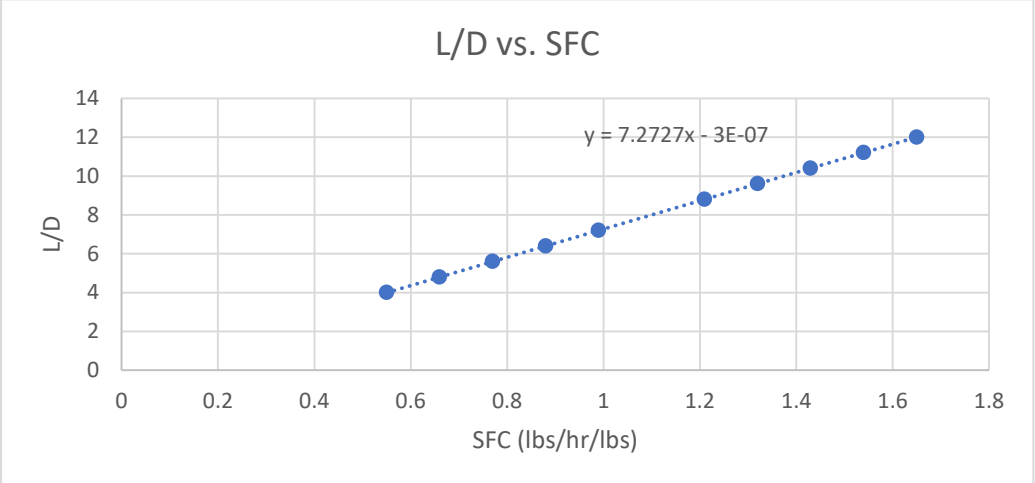

Figure 11. *SFC vs. L/D Trade Study*

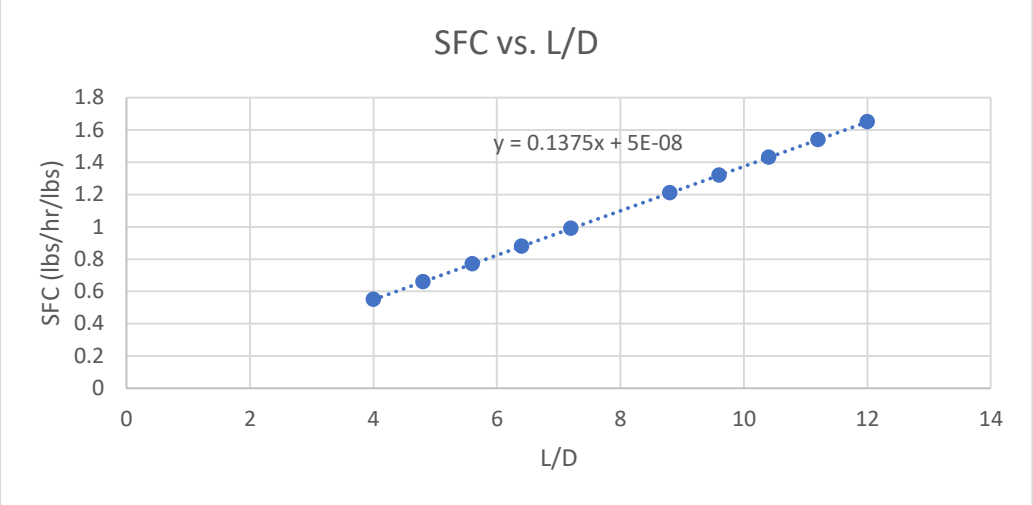

Discussion

In Table 3, the results from the studies done in this chapter are documented. Overall, the takeoff weight determined is within range for similar aircraft and therefore is acceptable.

The results found for each of the trade study plots will be discussed here. Figure 8 shows the results of changing the range and analyzing the resulting available payload change. This study shows that for every nautical mile increase, you must decrease the payload by 16.47 lbs. Figure 9 is the reverse of this study, payload is changed, and the resulting range is found. This study shows that for every pound increase in payload, the range must be decreased by 0.06 nautical miles. Figure 10 shows the results of changing the specific fuel consumption and finding the resulting lift to drag ratio. It showed that for every specific fuel consumption increase, the lift to drag ratio must increase by 7.27. Figure 11 is the reverse of the previous study changing the lift to drag ratio. It showed for every lift to drag ratio increase, the specific fuel consumption must also be increased by 0.14.

Based on these studies, the payload has been decreased to 150 passengers which allows the range to be increased to 4,533.7 NM. The cruise lift to drag ratio has also been increased to 10, which would increase the specific fuel consumption to 1.375 lbs/hr/lbs. The SFC is still reasonable so the increased lift to drag ratio will enhance the performance of the aircraft.

Table 3. *Important Parameters Determined in this Chapter*

Parameters Determined or Changed in this Chapter	
Parameter	**Value**
Takeoff Weight	352,000 lbs
Empty Weight	162,000 lbs
Fuel Weight	146,009 lbs
Fuel Fraction	0.5936
Payload	150 passengers
Range	4,534 NM

Performance Constraint Analysis

The purpose of this section is to determine the design point of the aircraft performance constraints. Determining performance constraints allows us to calculate the wing loading and thrust to weight ratio necessary for the intended specifications. This SST design falls under the Federal Aviation Regulation 25 for stall speed, takeoff/landing distance, climb, and maneuvering constraints. Also, in this section, the required propulsion system will be determined.

Based on FAR 25, the aircraft being designed needs to be sized to the takeoff/landing distance requirements as well as climb, and speed constraints.

Manual Calculation of Performance Constraints

This section details the hand calculations for the performance requirements given by FAR 25. Each calculation results in the relationship between wing loading and thrust to weight ratio that will be used for the matching plots.

Stall speed

$V_s = 150\ kts$ ("CONCORDE SST," 2003)

$$V_s = \sqrt{\frac{2(W/S)}{\rho C_{L_{max}}}} \longrightarrow 150\ kts = \sqrt{\frac{2(W/S)}{\left(2.26E-4\frac{slugs}{ft^3}\right)(1.5)}} \longrightarrow (W/S)$$

$$= 105.6\ psf$$

Takeoff distance

$$s_{TOFL} < 5000\ ft\ at\ 8000\ ft\ standard\ atmosphere$$

$$s_{TOFL} = 37.5 TOP_{25} \longrightarrow TOP_{25} = \frac{5000}{37.5} = 133.3\ psf$$

$$at\ 8000\ ft, \sigma = 0.786$$

$$TOP_{25}\sigma = \frac{(W/S)}{C_{L_{max}}(T/W)} \longrightarrow (133.3)(0.786) = \frac{(105.6)}{(1.5)(T/W)} \longrightarrow (T/W)$$

$$= 0.67$$

$$Relationship: (W/S) = 157.2(T/W)$$

$$s_{TOFL} < 5000\ ft\ at\ sea\ level$$

$$s_{TOFL} = 37.5TOP_{25} \longrightarrow TOP_{25} = \frac{5000}{37.5} = 133.3\ psf$$

$$at\ sea\ level, \sigma = 1$$

$$TOP_{25}\sigma = \frac{\left({}^{W}/_{S}\right)}{C_{L_{max}}\left({}^{T}/_{W}\right)} \longrightarrow (133.3)(1) = \frac{(105.6)}{(1.5)\left({}^{T}/_{W}\right)} \longrightarrow \left({}^{T}/_{W}\right) = 1.89$$

$$Relationship: \left({}^{W}/_{S}\right) = 199.95\left({}^{T}/_{W}\right)$$

Landing distance

$$s_{TOFL} = 5000\ ft\ at\ sea\ level$$

$$V_A = 1.3V_{SL}\ and\ V_{SL} = 0.3V_A^2$$

$$V_A = \sqrt{\frac{5000}{0.3}} = 129.1\ kts\ and\ V_{SL} = \frac{129.1}{1.3} = 99.3\ kts$$

$$\frac{2\left({}^{W}/_{S}\right)_L}{0.002378C_{Lmax_L}} = (99.3 * 1.688)^2 = 28100 \longrightarrow \left({}^{W}/_{S}\right)_L = 33.4C_{Lmax_L}$$

$$\left({}^{W}/_{S}\right)_{TO} = \frac{33.4}{0.85}C_{Lmax_L} = \frac{33.4}{0.85}(1.7) = 66.8\ psf$$

$$Relationship: \left({}^{W}/_{S}\right)_{TO} = 39.3C_{Lmax_L}$$

Drag polar estimation

$$\log S_{wet} = c + d * \log W_{TO}\ \ where\ c = -1.1868\ and\ d = 0.9609$$

$$\log f = a + b * \log S_{wet}\ \ where\ a = -2.5229\ and\ b = 1$$

$$W_{TO} = 352000\ lbs\ so, S_{wet} = 14348.45, and\ f = 43.043$$

$$C_{D_0} = \frac{f}{S} = 0.01116$$

$$Assume\ A = 2\ and\ e = 0.85$$

$from\ Roskam\ and\ changes\ with\ flaps\ and\ landing\ gear\ as\ follows$: (Roskam, 2003)

$$take\ off\ flaps: \Delta C_{D_0} = 0.015, e = 0.77$$

$$landing\ flaps: \Delta C_{D_0} = 0.065, e = 0.73$$

$$landing\ gear: \Delta C_{D_0} = 0.020, e = n/a$$

$$Drag\ polars:$$

$$clean, low\ speed: C_D = 0.0112 + 0.0374C_L^2$$

$$take\ off, gear\ up: C_D = 0.0262 + 0.0413C_L^2$$

$$take\ off, gear\ down: C_D = 0.0462 + 0.0413C_L^2$$

$$landing, gear\ up: C_D = 0.0762 + 0.0436C_L^2$$

$$landing, gear\ down: C_D = 0.0962 + 0.0436C_L^2$$

Climb constraints

Table 4. *FAR 25 Climb Requirements*

FAR 25 Climb Requirements			
For Takeoff Climb			
1. FAR 25.111	CGR > 0.012	Gear up, take off flaps	$V = 1.2V_{STO}$
2. FAR 25.121	CGR > 0	Gear down, take off flaps	$V = 1.1V_{STO}$
3. FAR 25.121	CGR > 0.024	Gear up, take off flaps, no ground effects	$V = 1.2V_{STO}$
4. FAR 25.121	CGR > 0.012	Gear up, flaps up, max cont. thrust	$V = 1.25V_{STO}$
For Landing Climb			
5. FAR 25.119	CGR > 0.032	Gear down, landing flaps	$V = 1.3V_{SL}$
6. FAR 25.121	CGR > 0.021	Gear down, approach flaps	$V = 1.5V_{SA}$

$$\left({}^{T}/_{W}\right) = 2\left[\frac{1}{{}^{L}/_{D}} + CGR\right]$$

$$For\ Climb\ Requirement\ 1\ at\ V_2 = 1.2V_{STO}$$

$$C_{L,TO,max} = \frac{1.5}{1.2^2} = 1.042$$

$$C_D = 0.0262 + \frac{C_L^2}{24.2} = 0.071$$

$$So, \frac{L}{D} = \frac{1.042}{0.071} = 14.68$$

$$\left({}^{T}/_{W}\right) = 2\left[\frac{1}{14.68} + 0.012\right] = 0.16$$

$$Correcting\ for\ Temperature: \frac{0.16}{0.8} = \left({}^{T}/_{W}\right) = 0.2$$

Speed constraints

$$Cruise\ Speed: V = 1720.7\ kts$$

$$\left({}^{T}/_{W}\right)_{req} = \frac{qC_{D_0}}{\left({}^{W}/_{S}\right)} + \frac{\left({}^{W}/_{S}\right)}{\pi Aeq}$$

$$Relationship: \left({}^{T}/_{W}\right)_{req} \frac{253.63}{\left({}^{W}/_{S}\right)} + 2.135E-5\left({}^{W}/_{S}\right)$$

Summary of performance constraints

Figure 12 shows the design point that was chosen, and the simplified matching plot that contains only one lift coefficient line per constraint. Table 5 shows the results gained from these studies. Maximum lift coefficients, stall

speed, aspect ratio, wing area, and thrust required were determined and will be used for further design.

Figure 12. *Matching Plot with Final Parameters*

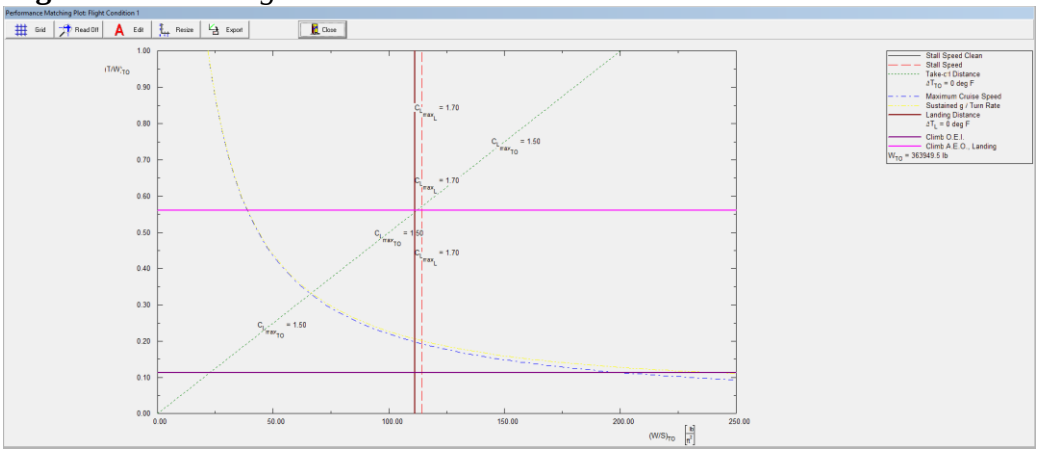

Table 5. *Performance Sizing Results*

Performance Sizing Results			
$C_{L_{TO}}$	1.5	AR	2
C_{L_L}	1.7	S	3,200 ft^2
V_S	150 kts	T	197,120 lbs
$(W/S)_{TO}$	110	W_{TO}	352,000 lbs
$(T/W)_{TO}$	0.56		

Selection of Propulsion System

Selection of the Propulsion System Type

This SST Design will cruise at Mach 3 at 60,000 ft altitude. These requirements dictate that an afterburning turbojet be used as a propulsion system like that used by the Concorde. While these requirements are currently at the edge of the design envelope for afterburning turbojet engines, in the years it would take to finish manufacturing of this aircraft, these engines should be more equipped to handle these requirements.

Selection of the Number of Engines

The takeoff thrust required by each engine was determined in the previous section to be 197,120 lbs. 6 engines would accommodate this at a very reasonable 32,853 lbs. each. If the design envelope for current afterburner turbojet engines were expanded, only 4 engines would be needed at 49,280 lbs. each. This aircraft will have four afterburner turbojet engines on top of the inner wing at the rear of the fuselage with a ramp inlet and exhaust in a balanced configuration.

Discussion

The manual calculations produced are within an acceptable range of that produced by the AAA program. It is known that the design point must be above the takeoff distance, cruise speed, maneuverability, and climb lines in the matching plot. The design point must also be to the left of the landing distance and stall speed lines. These requirements, designated by the FAR 25 certification, led to a point on the matching plot where a few parameters would be deemed critical. In this situation the critical parameters are: climb (landing) with all engines out, landing distance, and takeoff distance. These parameters all meet at a point on the matching plot that has been determined to be the design point. This implies that if any if these critical parameters are changed, the wing loading and thrust to weight ratio would change extensively.

The idea of the design point is to have a moderate wing loading with a thrust to weight ratio that is as low as possible to reduce the required wing size and thrust required. Wing area is determined from the wing loading ratio given the takeoff weight determined in the previous chapter. Thrust is also determined using the previously determined takeoff weight in the thrust to weight equation. The wing area and thrust determined by the matching plot agrees with that of the Concorde and therefore are taken to be reasonable.

At this point in the design, the following parameters have been determined to be critical or have the potential to have a major impact on the design:

- Range (from Trade Studies)
- Payload (from Trade Studies)
- AEO landing
- Landing Distance
- Takeoff Distance

Wing & Lateral Control Design

The purpose of this chapter is to design the wing and high lift devices to achieve the maximum lift coefficient required for all stages of flight. Most of the wing geometry has already been determined such as the aspect ratio and wing area. Items that remain to be decided are sweep angle, thickness ratio and airfoil shape. The wing geometry will give us a base value for our lift coefficient. The high lift devices are designed to push that value to the maximum needed for takeoff, landing and cruise.

Wing Planform Design

Previously, the gross wing area as well as the aspect ratio of the wing was determined.

$S = 3{,}308.6$ sq. ft.

AR = 2

The taper ratio of this design was determined from a similar aircraft (Concorde) to be λ=0.12. This aircraft will also have no dihedral as delta wings have inherent lateral stability and therefore usually lack a dihedral. The following calculations were done to determine sweep angle and thickness ratio (Roskam, 1997).

$$C_{root} = \frac{2 * S}{b(1+\lambda)} = 72.63\ ft$$

$$C_{tip} = \lambda * C_{root} = 8.72\ ft$$

$$mac = \left(\frac{2}{3}\right) C_{root} \left(\frac{1+\lambda+\lambda^2}{1+\lambda}\right) = 49.04\ ft$$

$$spanwise - mac = \left(\frac{b}{6}\right) \frac{1+2\lambda}{1+\lambda} = 15.01\ ft$$

$$L_{LE} = 90 - \arcsin\left(\frac{1}{M}\right) = 70.53\ deg$$

Note: While this is the leading-edge sweep angle that is calculated, a historical trend plot in Raymer's Aircraft Design indicates a leading-edge angle of 60 deg has been sufficient and so that is what will be used initially. Also, from Raymer's Aircraft Design, a thickness ratio (t/c) was determined to be 0.04, provisionally (Raymer, 2012).

Sweep Angle - Thickness Ratio Trade Study

To conduct a trade study between sweep angle and thickness ratio, a relationship was found between those two parameters to be (Ciornei, 2005):

$$^{t}/_{c} = 0.7185 + 3.107E - 5L - 0.1298C_L - 0.7210M_{DD}, where\ C_L = 1.8$$

A relationship between sweep angle, thickness ratio, and wing weight was also found (Ciornei, 2005):

$$W_{wing} = 0.0017(W_{TO} - W_F)\left(^{b}/_{\cos L_{\frac{1}{2}}}\right)^{0.75} * [1 + \left(\frac{6.3\cos L_{\frac{1}{2}}}{b}\right)^{\frac{1}{2}} * n_{ult}^{0.55} * \left(\frac{bS}{t_r(W_{TO} - W_F)\cos L_{\frac{1}{2}}}\right)^{0.3}, where\ t_r = {}^{t}/_{c} * C_{root}, and\ n_{ult} = 1$$

The trade study demonstrated in Figure 13, led to an aft sweep angle of 51.5 degrees and a thickness ratio of 0.03. As seen in the figure, the wing weight varies almost undetectably at this small of a thickness ratio, meaning, there is no need to consider its variation for this trade study.

Figure 13. *Thickness Ratio vs. Sweep Angle Trade Study*

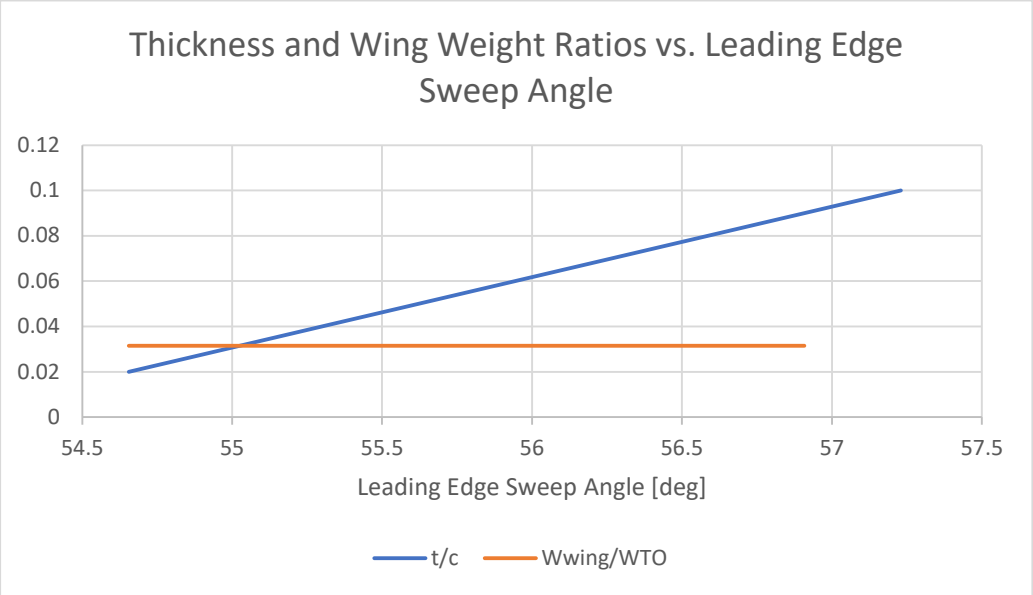

Airfoil Selection

Supersonic aircraft currently tend to choose airfoils simply as starting points for custom design of that aircraft's specific requirements. For the sake of simplicity, as airfoil design is not the focus of this report, an airfoil was chosen with no custom modifications which implies that its performance may not be as good as those in production. The airfoil chosen is the NACA 64A-203. The supercritical airfoils were designed for supersonic flight but also to perform well at high subsonic flight which will be important for takeoff and landing.

The equation used for angle of incidence (Roskam, 1997):

$$i = \frac{C_{L,CR}}{C_{L,\alpha}} + \alpha_0 = 16.42\ deg$$

This angle of incidence will help performance during subsonic flight but will need to be corrected for during supersonic flight was a twist. The wing needs to be as flat as possible during supersonic cruise for greatest performance. For this reason, and due to historical trends, a twist angle of -10 degrees was chosen.

Wing Design Evaluation

Using AAA, the rest of the wing geometries were determined from the aspect ratio, wing area, and leading-edge sweep angle.

Figure 14. *Wing Parameters from AAA*

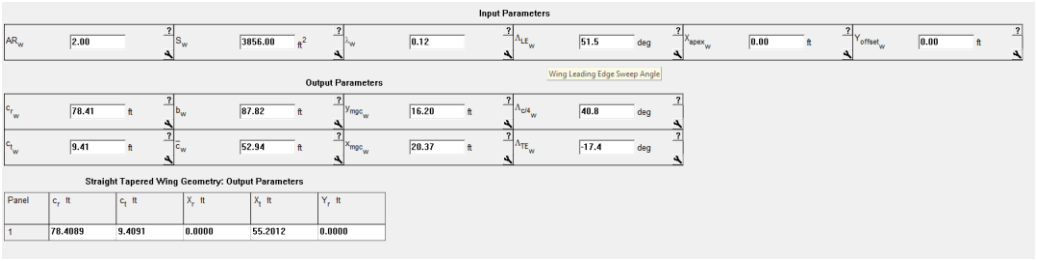

Design of High Lift Devices

From previous chapters, the maximum lift coefficient variables for the different stages of flight are known.

$$C_{L,\max TO} = 1.5$$
$$C_{L,\max L} = 1.7$$
$$C_{L,\max clean} = 1.8$$

Due to the high performance of delta wings, no high lift devices are needed to reach the lift coefficient values during any stage of flight. This is proven by the Concorde's and Tu-144's lack of high lift devices. This is simply an advantage that comes with this wing shape. An attempt at this analysis was conducted in AAA, though AAA states that some of its calculations are not suited for supersonic flight in this section. One example is that it cannot accept thickness ratios less than 6% although for supersonic flight this is very common. Going through the calculations with the simplifications that AAA makes to accommodate for these things yields a CLmax of 1.13. This is a bit lower than expected but it is expected that has to do with the program not being suited for this flight speed and the major edits to design points made to accommodate its equations. Based on the previous SST's lack of high lift devices, none will be designed here.

Figure 15. *Wing Max Lift Coefficient from AAA*

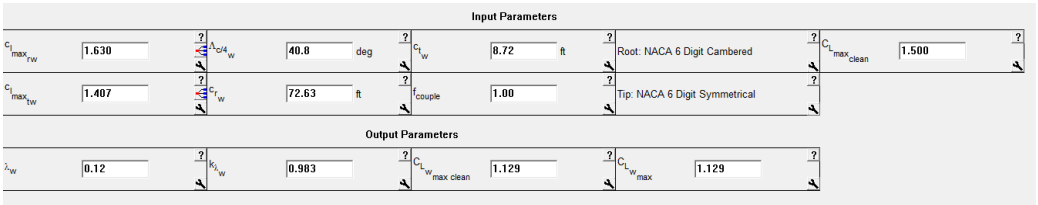

Design of Lateral Control Surfaces

Lateral control surface design is based on two reference aircraft: the Concorde and Tu-144. Both aircraft had elevons at the wing trailing edge. Elevons control pitch and roll on the same surface. If both surfaces are moved in the same direction, a pitch occurs. If each surface is moved in a different direction, a roll occurs. Given that this aircraft will have a V-Tail (discussed in

the next section), the elevator part of this is not needed. Therefore, this aircraft will have 2 ailerons at the trailing edge at 420 sq. ft. each.

Drawings

Figure 16. *Wing Geometry*

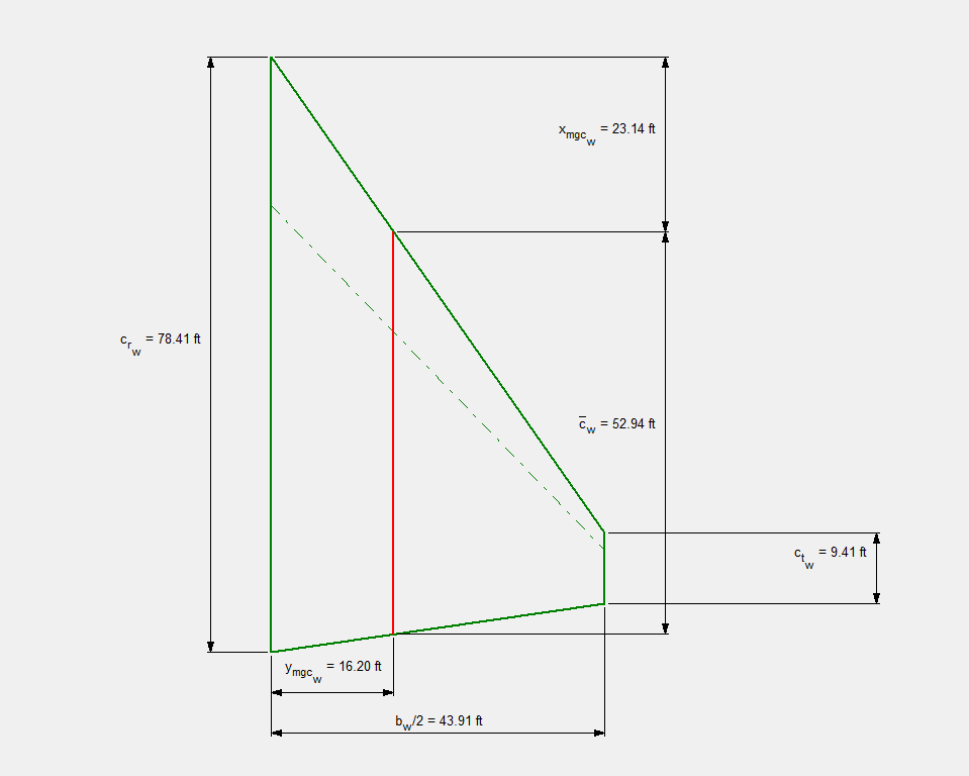

Discussion

Using the wing area and aspect ratio previously determined, the geometry of the wing was found to be similar to that of the Concorde. While supersonic aircraft usually custom make airfoils for the wings, this design was simplified by choosing a standard airfoil which may reduce performance. An evaluation of the wing's performance was attempted in AAA and subsequently abandoned when it became clear that the software did not support parameters used in supersonic flight. It was assumed that, given the similarities between the wing size and planform between this aircraft and the Concorde, the wing design is sufficient. Also related to the Concorde are the lack of high lift devices due to the inherent properties of the delta wing. Finally, ailerons were designed as the lateral control surface.

Figure 17. *Aircraft to Date*

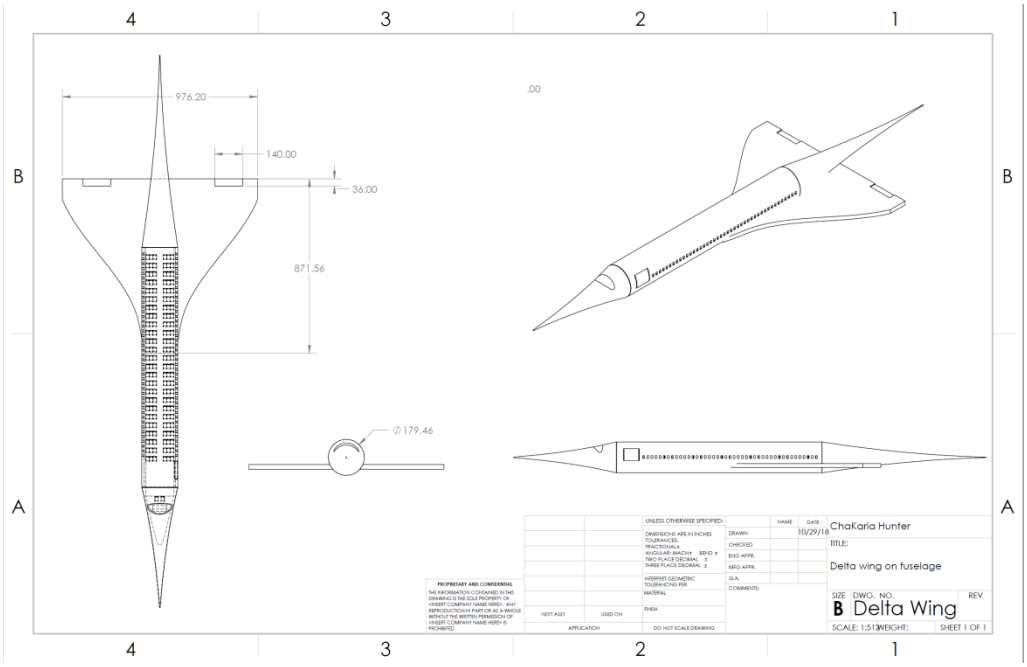

Empennage & Longitudinal/Directional Control Design

The purpose of this section is to design the empennage with its control surfaces to achieve the necessary control of the aircraft. A V-Tail will be designed for this aircraft instead of the conventional vertical fin. The V-Tail design provides smaller tail surfaces and reduced number of control surfaces thereby reducing drag. The geometry of a V-Tail is easily determined by first identifying the needed horizontal and vertical stabilizer areas and projecting them onto a defined angle. The control surface on a V-Tail is the combination of a rudder and elevator, termed a 'ruddervator'.

Overall Empennage Design

The empennage designed for this aircraft will be a V-Tail. The geometry will be based on that of the Concorde ("CONCORDE SST," 2003). The Concorde had one vertical fin and horizontal elevators. These will be combined to create the V-Tail. The empennage will sit just aft of the wing and on the outside of the engine with a distance between the two fins of 16.2 ft. The location can be described as: $x = -69\ ft, y = 9.85\ ft$. The size of the two fins will be determined by using the area of the vertical fin and the horizontal elevators: $S_h = 96.6\ sq.ft, S_v = 365\ sq.ft$. ("CONCORDE SST," 2003).

To determine the angle the fins will be at, an equation from Roskam is used (Roskam, 1997):

$$\zeta_v = \arctan\frac{S_v}{S_h} = 75.2\ deg$$

To determine what the area of each fin should be, the Pythagorean theorem is used (Roskam, 1997):

$$S_{VT} = \sqrt{S_h^2 + S_v^2} = \frac{377.6}{2} = 188.8\ sq.ft\ each$$

Design of The V-Tail

V-Tails are not conventional empennage choices for supersonic aircraft. This is because a delta wing is usually employed and therefore a horizontal stabilizer is not completely necessary. In this case, the V-Tail is used to keep the wing design simple by using a simpler aileron and making the tail more complex by use of a ruddervator. Given the uniqueness of this situation, there is no historical data for this design at supersonic speeds. Instead, a general idea was gathered about acceptable geometry parameters from Raymer's Aircraft Design (Raymer, 2012) and different combinations were analyzed using the AAA software.

Historically, supersonic aircraft have a vertical stabilizer with an aspect ratio of less than 2. An attempt the apply this trend to the V-Tail with the area remaining fixed, created a tail that spanned about half the length of the aircraft. This being unacceptable, a sweep was done of the aspect ratios until a reasonable geometry was found. From this analysis, the aspect ratio of the V-Tail was set at AR = 5. The taper ratio was then derived from that of aircraft with a similar tail aspect ratio. It was set at λ = 0.4. The sweep angle was harder to find comparable data for, so the tail sweep angle of the Concorde was used and $\Lambda_{LE-Tail}$ was set at 20 degrees. Following a suggestion from Raymer's Aircraft design, the thickness ratio was set to be 10% less than that of the wing at t/c = 0.027. Lastly, a symmetric NACA 5 series airfoil would be used and modified for thickness as none currently have the thickness required.

Empennage Design Evaluation

An evaluation of the previously described empennage design was conducted in the AAA program. This evaluation yielded more specific geometry parameters such as chord length at the root and tip, quarter chord and trail edge sweep angles, and mean aerodynamic chord lengths. These parameters were then used to determine the maximum clean lift coefficient for the tail fins. The CLmax found for this design was 0.732.

Figure 18. *Design of V-Tail in AAA*

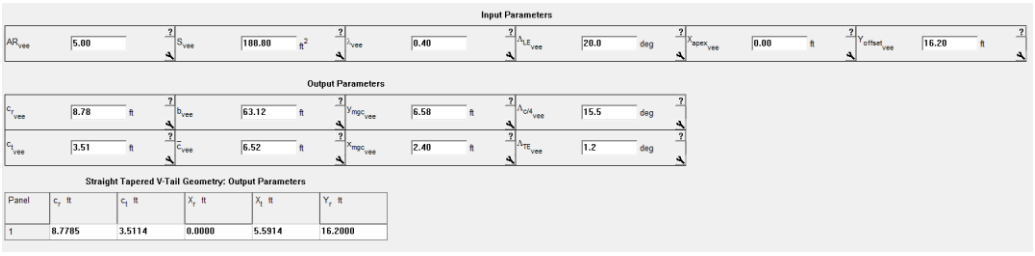

Figure 19. *V-Tail CLmax Analysis in AAA*

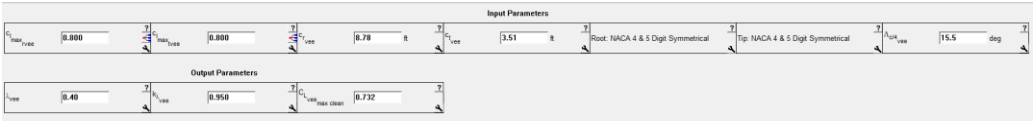

Design of the Longitudinal and Directional Controls

This aircraft will have one control surface for both longitudinal and directional controls: the ruddervator. The rudder, on its own, controls the yaw of the aircraft. The elevator controls the pitch. The idea of the V-Tail is to combine these two surfaces. Using the Concorde as a reference, the areas of these surfaces are: $S_h = 114.8\ sq.ft\ and\ S_{rudder} = 112\ sq.ft$. To find the projection needed for each of these surfaces on the V-Tail, the Pythagorean theorem is used (Roskam, 1997).

$$S_{ruddervator} = \sqrt{S_h^2 + S_{rudder}^2} = \frac{160.38}{2} = 80.2\ sq.ft\ each$$

Drawings

Figure 20. *V-Tail Fin Geometry*

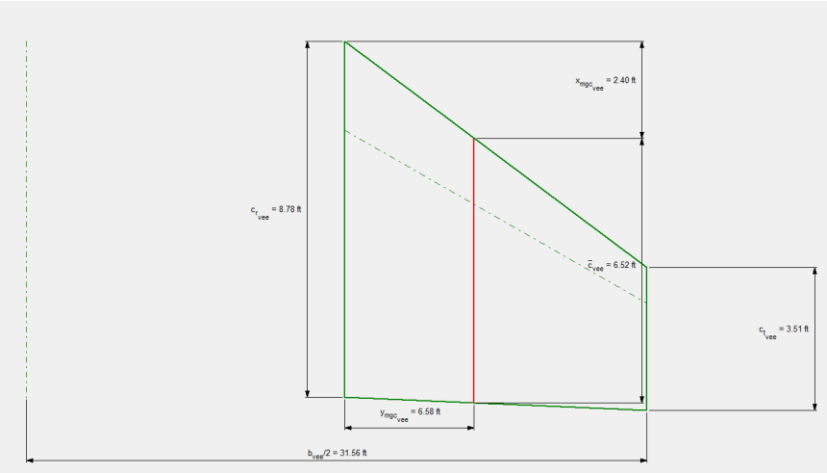

Discussion

Overall the design of the V-Tail was done as a projection of the horizontal stabilizer and elevators of the Concorde onto the angled surface. The AAA program could successfully determine the max lift coefficient of the tail even though it could not for the delta wing. This should be investigated further at a later time. The ruddervator was designed as a projection of the rudder and elevator onto the angled surface and the Pythagorean theorem was used to determine how much area was required for the combination of these surfaces. Overall, the geometries and performance values found are, at the very least, similar to that of the Concorde which instills confidence in the design.

Figure 21. *Full Aircraft Design to Date*

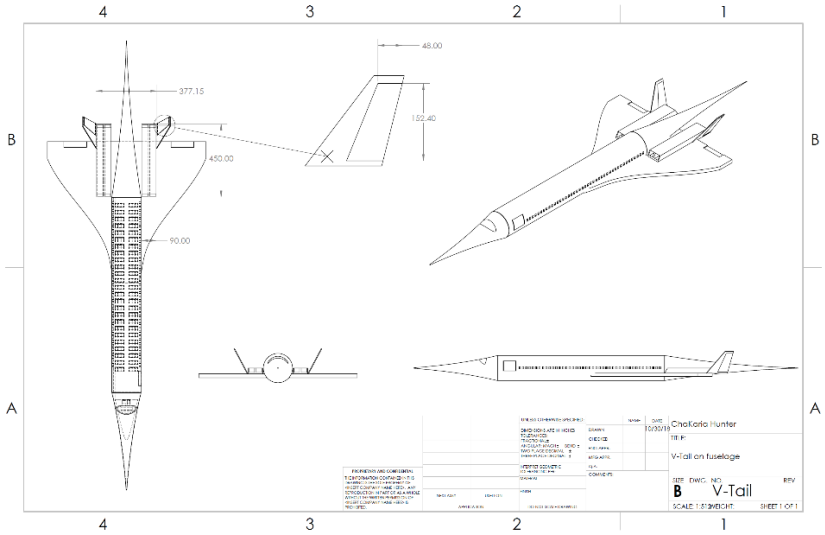

Landing Gear Design, Weight & Balance Analysis

The purpose of this section is to initially estimate the center of gravity location of the aircraft as it is currently designed. This will aid in the placement and design of the landing gear. A component weight breakdown will be conducted in order to determine the center of gravity of each component of the aircraft. The center of gravity is important because it changes during flight and throughout that change, the aircraft must remain stable. For this purpose, a diagram of how the center of gravity of this specific plane changes at each phase of flight, is also presented in this section.

Estimation of the Center of Gravity Location for the Airplane

A component weight table was previously estimated in DAR Corporation's AAA program (Figure 22). This table was used in combination with estimated center of gravity locations for each of the component groups (Table 6). These two steps are first in finding the center of gravity of the whole aircraft which is required before design of the landing gear.

Figure 22. *Estimated Component Weight Table*

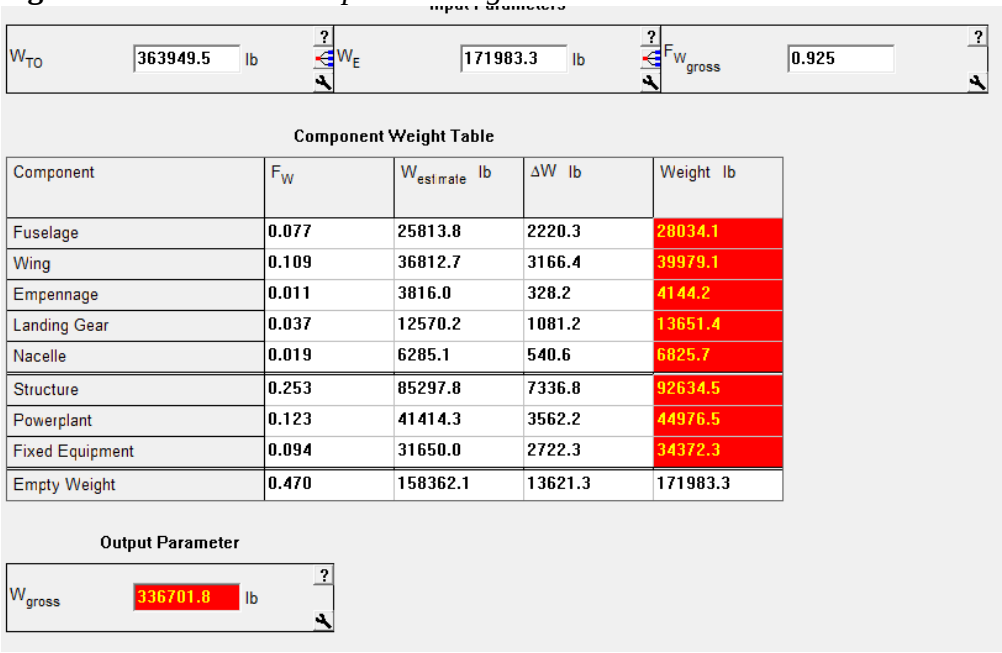

Table 6. *Component Weight and Center of Gravity Location*

Component	Weight [lbs]	CG Estimate(x-axis) [in]
Baggage	4680	851
Fuselage	28034	1380
Wing	39979	1924
Passengers	27300	1257
Fuel	146009	1593
Engines	51802	2026
Empennage	4144	2182
Landing Gear	13651	1665

Figures 23 and 24 show a representation of where each of the component centers of gravity lies with respect to each other on the aircraft and the calculation of the longitudinal center of gravity. Figure 24 displays the CG location of the aircraft.

Figure 23. *Current Aircraft Design with Component Weight Groups and General Locations*

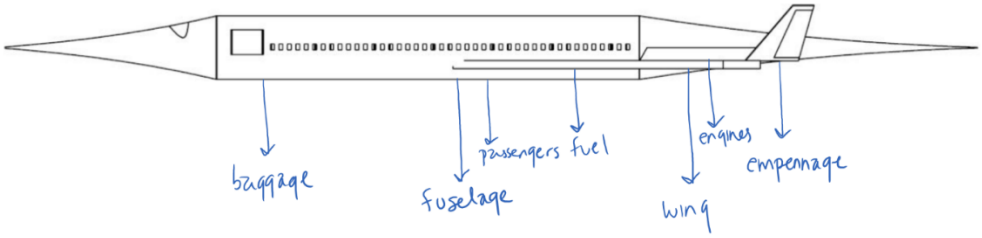

Figure 24. *Manual Calculations for Center of Gravity Location and Rear Landing Gear Location*

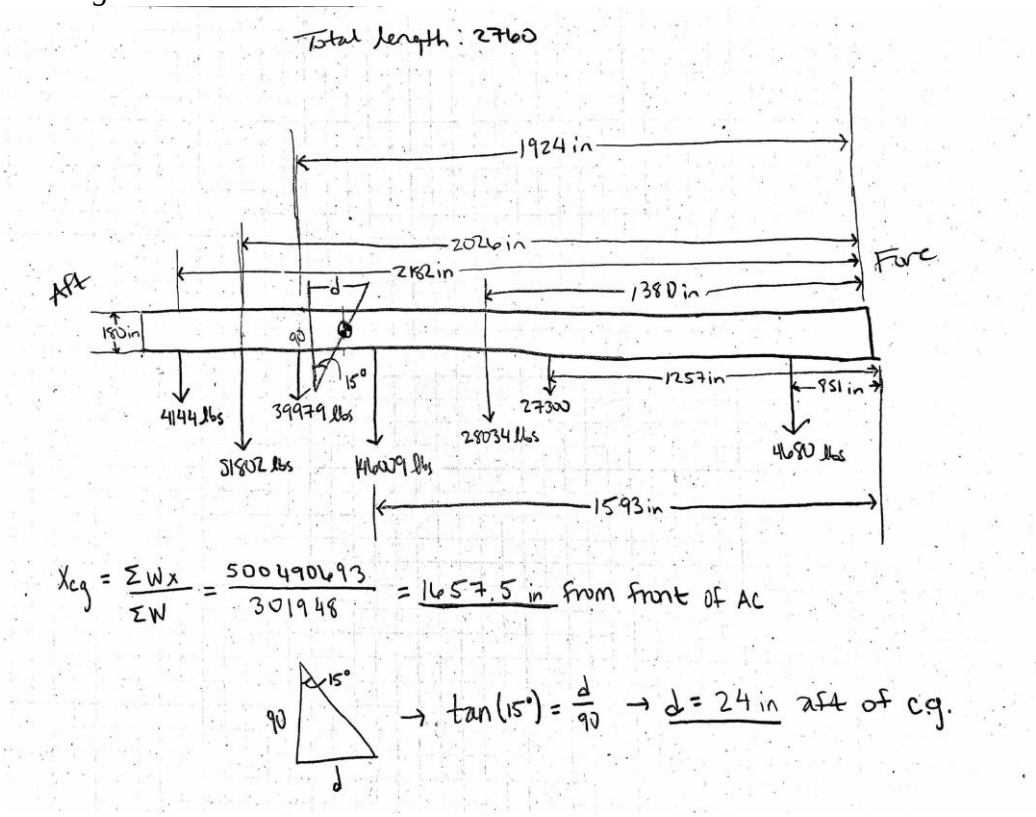

Landing Gear Design

This aircraft will have tricycle landing gear designed based on that of transport jets of a similar weight class based on Roskam's table of Typical Landing Gear Data (Roskam, 1997).

Table 7. *Typical Landing Gear Wheel Data from Roskam*

Table 9.2 Typical Landing Gear Wheel Data (n_s = 2 unless otherwise noted)

Type	W_{TO}	Main Gear $D_t$xb$_t$	Main Gear n_sP_m/W_{TO}	Main Gear PSI	Main Gear n_{mt}	Nose Gear $D_t$xb$_t$	Nose Gear P_n/W_{TO}	Nose Gear PSI	Nose Gear n_{nt}
	lbs	in.xin.				in.xin.			
Transport Jets	44,000	34x12	0.89	75	2	24x7.7	0.11	68	2
	73,000	40x14	0.92	77	2	29.5x6.75	0.08	68	2
	116,000	40x14	0.94	170	2	24x7.7	0.06	150	2
	220,000	40x14	0.94	180	4	29x7.7	0.06	180	2
	330,000	46x16	0.93	206	4	40x14	0.07	131	2
	572,000	52x20.5	0.93	200	4*	40x15.5	0.07	190	2
	775,000	49x17	0.94	205	4**	46x16	0.06	190	2
Military Trainers	2,500	17x6	0.82	36	1	13.5x5	0.18	28	1
	5,500	20.3x6.5	0.91	60	1	14x5	0.09	40	1
	7,500	20.25x6	0.92	65	1	17.2x5.0	0.08	45	1
	11,000	23.3x6.5	0.90	143	1	17x4.4	0.10	120	1
Fighters	9,000	20x5.25	0.86	135	1	17x3.25	0.14	82	1
	14,000	18.5x7	0.87	110	1	18x6	0.13	37	1
	25,000	24x8	0.91	210	1	18x6.5	0.09	120	1
	35,000	24x8	0.90	85	2	21.5x9.8	0.10	57	1
	60,000	35.3x9.3	0.88	210	1	21.6x7.5	0.12	120	2
	92,000	42x13	0.93	150	1	20x6.5	0.07	120	2

For Flying Boats, Amphibious and Float Airplanes as well as for Supersonic cruise airplanes, use jet transport data.

*three main gear struts: n_s = 3 ** four main gear struts: n_s = 4

Note: all other airplanes have n_s = 2: two main gear struts.

Main Gear

The static load per strut of the main gear is calculated and compared to that of the load ratio in Roskam's Table 9.2 (Table 7) (Roskam, 1997). The equations are determined from the geometry in Figure 25 provided by Roskam.

Figure 25. *Geometry for Landing Gear Load Calculations from Roskam*

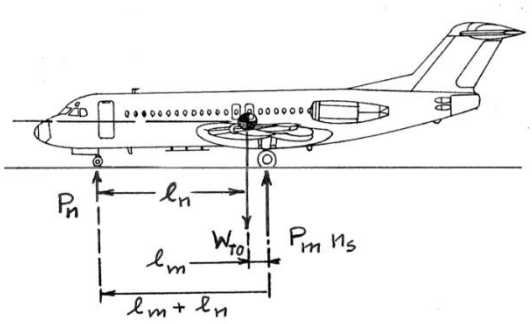

Figure 9.2a Geometry for Static Load Calculation for Tricycle Gears

$$P_m = \frac{W_{TO} l_n}{n_s(l_m + l_n)} \; where \; l_n = 757.5 \; in, l_m = 24 \; in, and \; n_s = 2.$$

$$P_m = 170{,}595 \; lbs$$

$$\frac{n_s P_m}{W_{TO}} = \frac{(2)(170{,}595)}{(352{,}000)} = 0.97$$

There will be two main gear struts with four tires each. Each tire diameter will be 46 inches with a thickness of 16 inches pressurized to 206 PSI. The strut diameter is estimated to be 10 inches.

Figure 26. *Main Landing Gear Drawing*

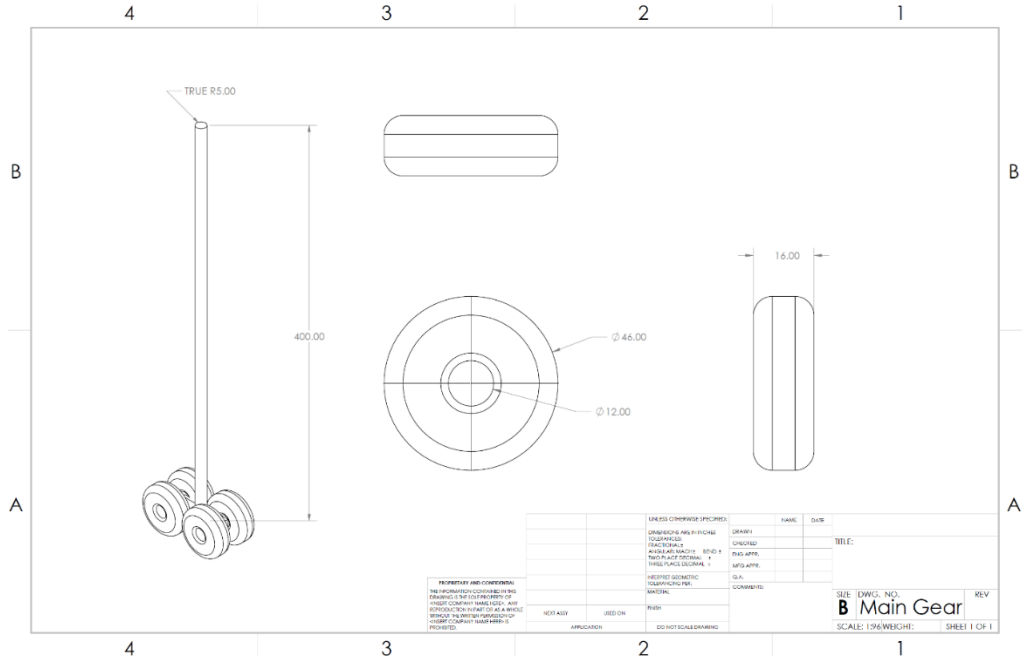

Nose Gear

Load ratios of the nose gear is calculated in this section to determine the design parameters.

$$P_n = \frac{W_{TO} l_m}{(l_m + l_n)} \; where \; l_n = 757.5 \; in \; and \; l_m = 24 \; in$$

$$P_m = 10{,}810 \; lbs$$

$$\frac{P_n}{W_{TO}} = \frac{(10{,}810)}{(352{,}000)} = 0.031$$

There will be one main gear strut with two tires. Each tire diameter will be 40 in with a thickness of 14 in pressurized to 131 PSI. The strut diameter is estimated to be 6 in.

Figure 27. *Nose Landing Gear Drawing*

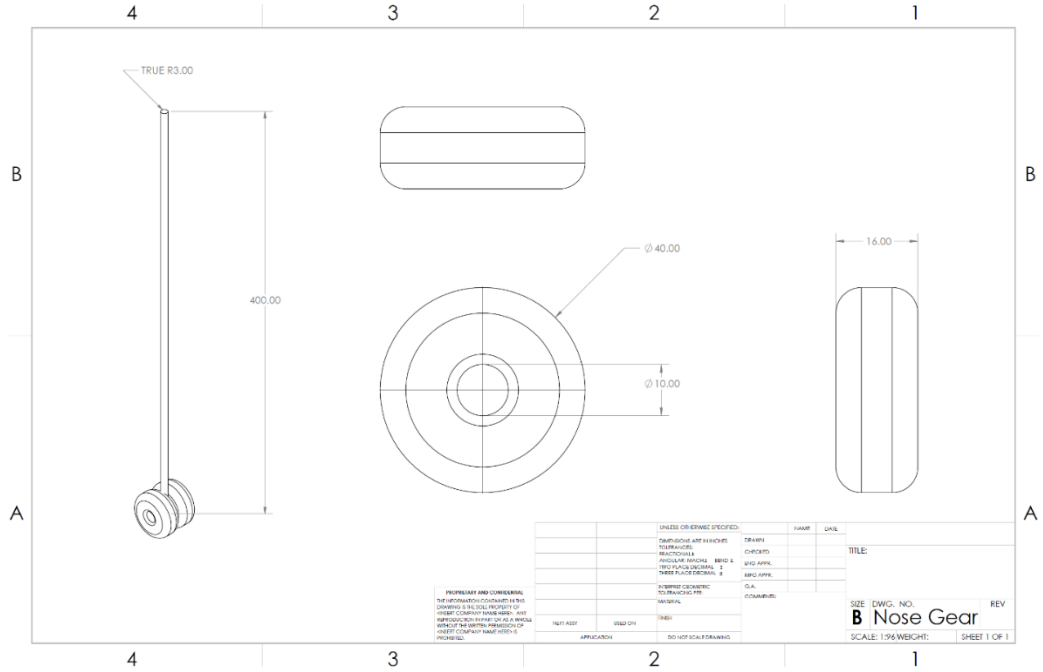

Preliminary Arrangement

Three different criteria are considered in the preliminary arrangement of the landing gear: tip-over criterion, longitudinal ground clearance, and lateral ground clearance.

The tip-over criterion provides the distance behind the center of gravity that the landing gear should be. A triangle can be formed between the center of gravity and the base of the landing gear with a minimum angle of 15 degrees. The distance behind the CG is found to be 24 in.

Figure 28. *Tip-Over Criterion*

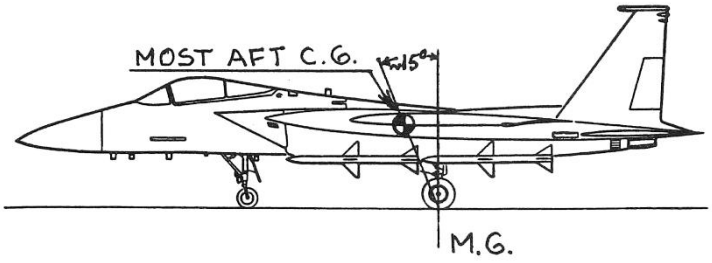

Longitudinal Tip-over Criterion for Tricycle Gears

The longitudinal ground clearance provides the minimum height of the landing gear struts. Knowing where the landing gear is placed along the x-axis of the plane, a triangle is formed with a minimum angle of 15 degrees from the

height of the tail as in Figure 29. The height of the struts is determined to be 450 in.

Figure 29. *Longitudinal Ground Clearance Criterion*

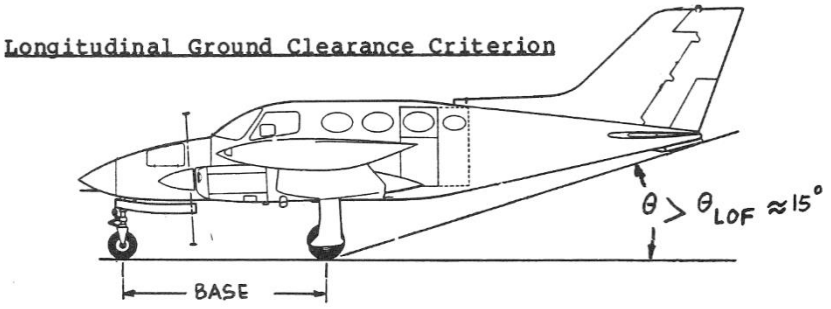

The lateral ground clearance determines the track width of the landing gear knowing the height of the wing. A triangle can be formed with a minimum angle of 5 degrees from the base of the tire to the lowest point on the wing. The track width is determined to be 60.8 in.

Figure 30. *Lateral Ground Clearance Criterion*

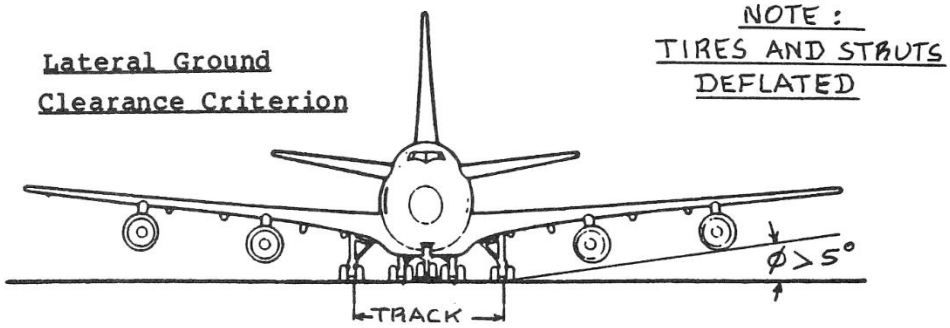

Weight and Balance

Component Weight Breakdown

A final component weight breakdown is determined by using the AAA program (Figure 31). The center of gravity of each component including the landing gear is used to determine the static center of gravity of the aircraft. After this analysis the tip-over criterion needed to be reevaluated. The angle between the base of the landing gear and the lowest point of the tail was determined to be greater than the minimum margin declared by Roskam and therefore acceptable to remain in the designed position.

Figure 31. *Weight Component Table from AAA Program*

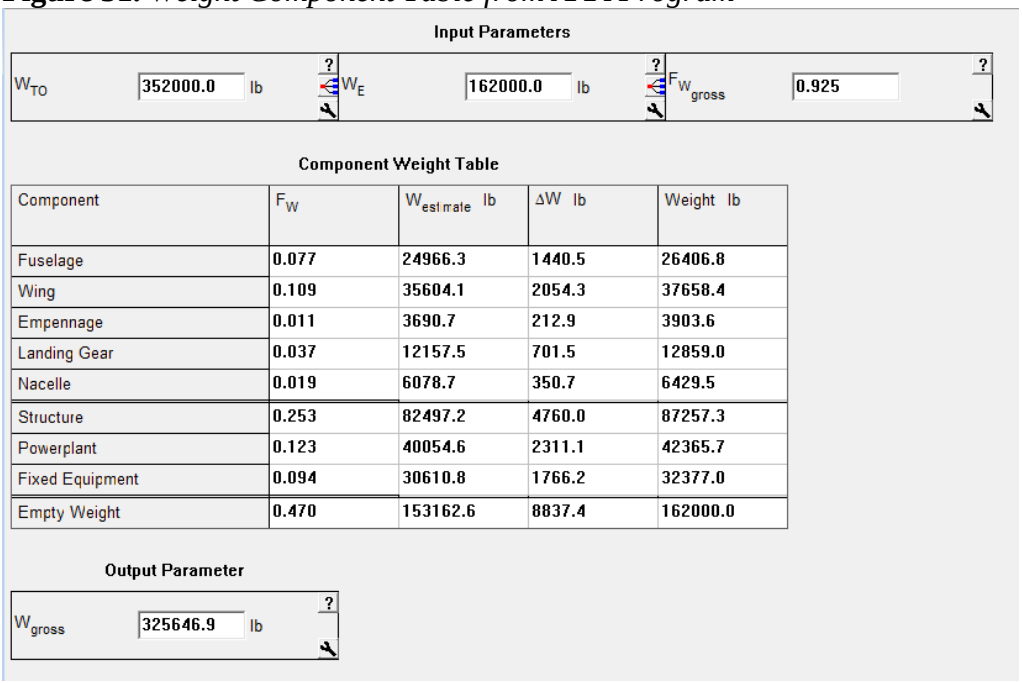

Input Parameters

W_{TO}	352000.0 lb	W_E	162000.0 lb	$F_{W_{gross}}$	0.925

Component Weight Table

Component	F_W	$W_{estimate}$ lb	ΔW lb	Weight lb
Fuselage	0.077	24966.3	1440.5	26406.8
Wing	0.109	35604.1	2054.3	37658.4
Empennage	0.011	3690.7	212.9	3903.6
Landing Gear	0.037	12157.5	701.5	12859.0
Nacelle	0.019	6078.7	350.7	6429.5
Structure	0.253	82497.2	4760.0	87257.3
Powerplant	0.123	40054.6	2311.1	42365.7
Fixed Equipment	0.094	30610.8	1766.2	32377.0
Empty Weight	0.470	153162.6	8837.4	162000.0

Output Parameter

W_{gross}	325646.9 lb

Table 8. *Center of Gravity Table for Current Design*

Component	Weight	X (from front of AC)	Y (from right of AC	WX	WY
Wing	37658.4	1343.38	488.1	50589541.39	18381065.04
V-Tail	3903.6	1976.59	488.1	7715816.724	1905347.16
Nacelles	6429.5	1694.84	488.1	10896973.78	3138238.95
Fuselage	26406.8	1380	488.1	36441384	12889159.08
Landing Gear	12859	1681.5	488.1	21622408.5	6276477.9
Baggage	4680	851	488.1	3982680	2284308
Passengers	27300	1257	488.1	34316100	13325130
Fuel	146009	1593	488.1	232592337	71266992.9
Engines	51802	2026	488.1	104950852	25284556.2
Totals	317048.3			503108093.4	154751275.2
	CG Direction	Inches			
	Xcg	1586.849995			
	Ycg	488.1			

Center of Gravity Location for Various Loading Scenarios

The CG excursion diagram is formed to determine how the center of gravity shifts during all phases of flight. This will determine if the static CG of the aircraft is in the correct position. The CG excursion diagram formed for this aircraft is shown in Figure 32.

Figure 32. *Center of Gravity Excursion Diagram*

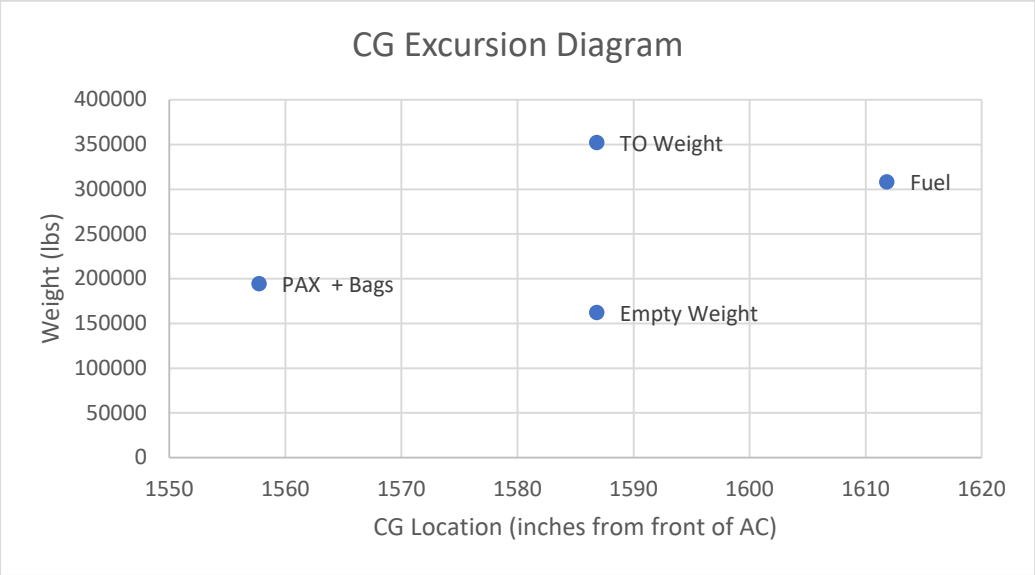

Discussion

The preliminary arrangement and dimensions of the landing gear are determined in this chapter to be as shown in the complete aircraft drawing below. The arrangement is designed based on center of gravity location of the aircraft and the dimensions are based on historical data from aircraft of a similar weight class. Lastly the excursion diagram was formed to analyze the shift of the CG during different phases of flight. The excursion diagram proved the CG location determined to be acceptable for this type of aircraft as stated by Roskam's Table of Center of Gravity Ranges in Figure 33.

Figure 33. *Center of Gravity Ranges from Roskam*

Table 10.3 Examples of Center of Gravity Ranges

Type	C.G. Range (in.)	C.G. Range $fr.\bar{c}_w$	Type	C.G. Range (in.)	C.G. Range $fr.\bar{c}_w$
Homebuilts	5	0.10	Military Trainers	8	0.10
Single Engine Prop. Driven	7-18	0.06-0.27	Fighters	15	0.20
Twin Engine Prop. Driven	9-15	0.12-0.22	Mil.Patr. Bomb and Transp.	26-90	0.30
Ag. Airpl.	5	0.10	Fl.Boats,	7-28	0.25
Business Jets	8-17	0.10-0.21	Amph. and Float		
Regional TBP	12-20	0.14-0.27	Amph. and		
Jet Transp.	26-91	0.12-0.32	Supersonic Cruise	20-100	0.30

Figure 34. *Landing Gear Drawing*

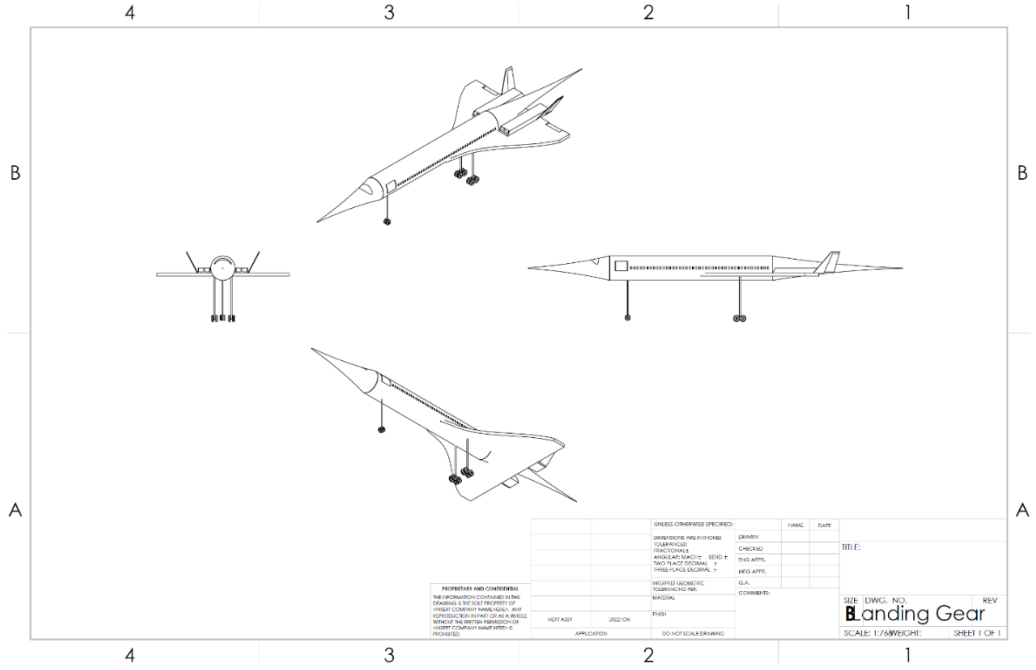

Stability & Control Analysis

The purpose of this section is to determine if the aircraft as designed is longitudinally and directionally stable. Longitudinal stability is based on the size of the horizontal stabilizer. Directional stability is based on the size of the vertical stabilizer. For this aircraft, the horizontal and vertical stabilizers are taken to be the respective projections of the V-Tail. Determining whether the vehicle is stable will tell if there is a tip over problem or problem with the center of gravity travel. The last requirement that will be addressed is the minimum control speed requirement for a one engine out scenario.

Static Longitudinal Stability

Longitudinal stability is determined by resizing the projection of the V-Tail onto the horizontal and investigating the subsequent aerodynamic center and center of gravity travel along the longitudinal axis of the aircraft. This aircraft is required to have ‘de-facto’ stability according to Roskam (Roskam, 1997). Therefore, the minimum static margin between the center of gravity and the aerodynamic center is 5%. As shown in Figure 36, the static margin for this aircraft is -0.083 at a horizontal stabilizer area of 96.6 sq. ft. See the equations below from Roskam (Figure 35) used to create the aerodynamic center leg of the X-Plot. The center of gravity was adjusted from previous weight and balance calculations.

Figure 35. *Longitudinal Plot Equation from Roskam*

The a.c. leg is calculated with the following equations:

$$\bar{X}_{ac_A} = [\bar{X}_{ac_{wf}} + \{C_{L_{\alpha_h}}(1 - d\varepsilon_h/d\alpha)(S_h/S)\bar{X}_{ac_h} - C_{L_{\alpha_c}}(1 + d\varepsilon_c/d\alpha)\bar{X}_{ac_c}(S_c/S)\}/C_{L_{\alpha_{wf}}}]/F, \quad (11.1)$$

where:

$$F = [1 + \{C_{L_{\alpha_h}}(1 - d\varepsilon_h/d\alpha)(S_h/S) + C_{L_{\alpha_c}}(1 + d\varepsilon_c/d\alpha)(S_c/S)\}/C_{L_{\alpha_{wf}}}] \quad (11.2)$$

$$x_{ac_A} = \left[x_{ac_{wf}} + \frac{[C_{L_{\alpha h}}(1 - d\varepsilon_h/d\alpha)(S_h/S)x_{ac_h}]}{C_{L_{\alpha wf}}}\right]/F$$

$$F = 1 + \frac{[C_{L_{\alpha h}}(1 - d\varepsilon_h/d\alpha)(S_h/S)x_{ac_h}]}{C_{L_{\alpha wf}}}$$

$$\textbf{\textit{Given}}: S_h = 96.9\, ft^2, c_{vee} = 6.52, C_{L_{\alpha_w}} = 2\pi, S = 3308.6\, ft^2, C_{L_{\alpha_h}} = 2\pi, x_{ac_{wf}} = 0.926, y_{ac_{wf}} = 15.01, x_{ac_h} = 0.368$$

$$\textbf{\textit{Yields}}: \quad F = 1 + 1.5E - 4S_h$$

$$x_{ac_A} = \frac{0.926 + 5.56E - 5S_h}{1 + 1.51E - 4S_h}$$

Figure 36. *Longitudinal X-Plot*

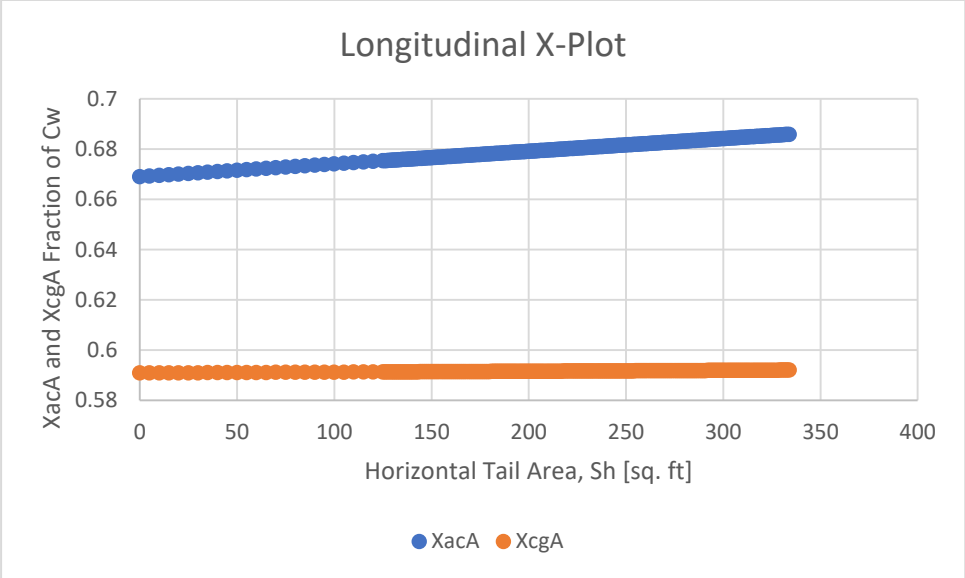

Static Directional Stability

Directional stability is determined by resizing the projection of the V-Tail onto the vertical and finding the sideslip produced. The required sideslip for de-facto stability is 0.001 per degree. As shown in Figure 37, the sideslip at the current design point is 0.000014 per degree. Based on this, the required sideslip to rudder feedback gain is found to be -0.082 deg/deg.

$$C_{n_\beta} = C_{n_{\beta_{wf}}} + C_{L_{\alpha_v}}(\frac{S_V}{S})(\frac{x_V}{b})$$
$$C_{n_\beta} = -0.004 + (1.115E-5)S_V$$
$$\Delta C_{n_\beta} = 0.001 - 0.000014 = 9.86E-4$$
$$k_\beta = \frac{\Delta C_{n_\beta}}{C_{n_{\delta_r}}} = \frac{9.86E-4}{-0.012} = -0.082\ deg/deg$$

Figure 37. *Directional X-Plot*

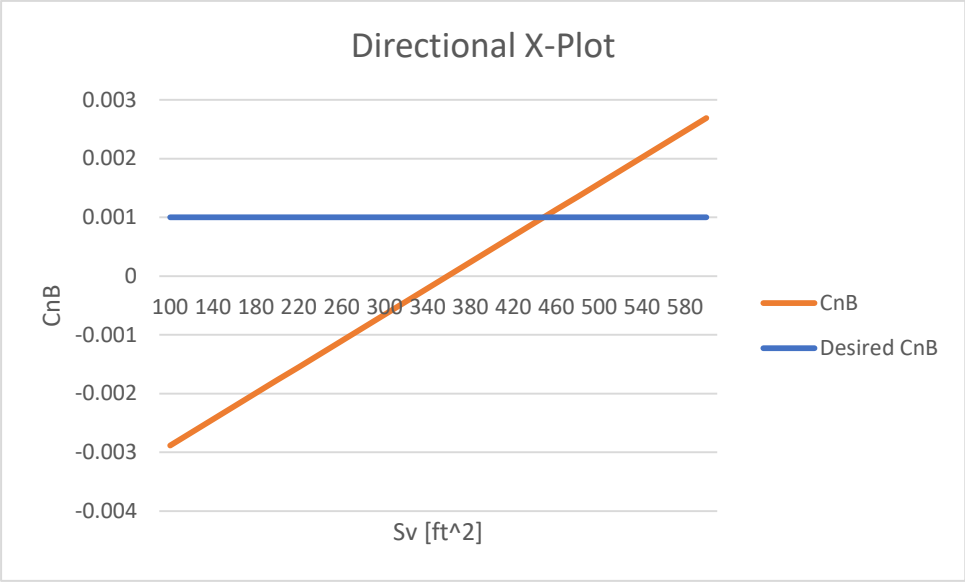

<u>One Engine Out Requirement</u>

From a previous section, it is known that the takeoff thrust required for each engine in 49,280 lbs. The lateral distance of the farthest engine from center line is found to be 135 inches from the previous drawings. These parameters are used to calculate the rudder deflection requirement. The maximum allowable rudder deflection is 25 degrees. For this aircraft, it is found to be -22.7 degrees.

$$N_{t_{crit}} = T_{TO_e} y_t = (49{,}280\ lbs)(135\ in) = 6652800\ in - lbs$$
$$N_D = 0.25 N_{t_{crit}} = 1663200\ in - lbs$$
$$V_{mc} = 1.2V_s = (1.2)(150\ kts) = 180\ kts$$

$$\delta_r = \frac{N_D + N_{t_{crit}}}{q_{mc} S b C_{n_{\delta_r}}} = -22.7\ degrees$$

Empennage Design – Weight & Balance – Landing Gear Design – Longitudinal Static Stability & Control Check

Based on the stability and control analysis completed in this chapter it is determined that there is no tip-over problem, center of gravity travel issue, or most critical engine velocity problem. There is however a longitudinal stability issue. The static margin is outside of the minimum allowable for de-facto stability aircraft but within range for inherent stability aircraft. Therefore, it is believed that this is a repairable problem. The horizontal stabilizer simply needs to be smaller. The directional stability is not perfect but is within correctable range for the rudder.

Discussion

From the longitudinal stability analysis, it was found that the horizontal stabilizer needs to be made smaller in area. This finding makes sense because previous supersonic transports such as the Concorde did not have horizontal stabilizers because it is not necessary for stability with the delta wing. The attempt the incorporate a V-Tail into the design is creating a longitudinal stability flaw. Directional stability of this aircraft is within range of the rudder capability and is determined to be acceptable. The one engine out requirement for this aircraft is met.

Drag Polar Estimation

The purpose of this section is to present the relation between the lift and drag coefficients for this aircraft. This is done by first computing the wetted area of each component of the aircraft and using that to find the parasitic area based on historical data. From this information, the clean, zero lift drag coefficient can be determined for a low speed. This value is used with the low speed drag elements such as takeoff and landing flaps and landing gear to compute the drag polars.

Airplane Zero Lift Drag

In order to compute the aircraft zero lift drag, the wetted area of the aircraft must be accurately determined. Roskam presents methods for computing the wetted area of the individual elements of the aircraft such as the wing, fuselage, tail and engines. The total wetted area of the aircraft is then used to find the parasitic area for the calculation of the zero lift drag coefficient. The parasitic area is found based on historical data in Roskam (Roskam, 1997).

$$S_{wet_{wing}} = 6162.1\ ft^2$$
$$S_{wet_{fuselage}} = 42.02\ ft^2$$
$$S_{wet_{V-Tail}} = 761.87\ ft^2$$
$$S_{wet_{engine}} = 281.25\ ft^2$$
$$Total\ S_{wetted} = 7{,}247.24\ ft^2$$
$$f = 20\ ft^2$$
$$C_{D_0} = \frac{f}{S} = 0.006$$

Low Speed Drag Increments

Roskam presents historical data of many classes of aircraft for determining the drag increments for different flight conditions (Roskam, 1997). These are necessary as they add to the zero lift drag in the calculation of the drag polars.

Table 9. *Low Speed Drag Increments*

Condition	ΔC_D	e
TO Flaps	0.015	0.77
LND Flaps	0.065	0.73
LND Gear	0.020	n/a

Airplane Drag Polars

The drag polars for this aircraft have been recalculated here to replace that which is estimated previously.

$$Drag\ polars:$$
$$clean: C_D = 0.006 + 0.187C_L^2$$
$$take\ off, gear\ up: C_D = 0.021 + 0.207C_L^2$$
$$take\ off, gear\ down: C_D = 0.041 + 0.212C_L^2$$
$$landing, gear\ up: C_D = 0.071 + 0.218C_L^2$$
$$landing, gear\ down: C_D = 0.091 + 0.218C_L^2$$

Figure 38. *Drag Polar*

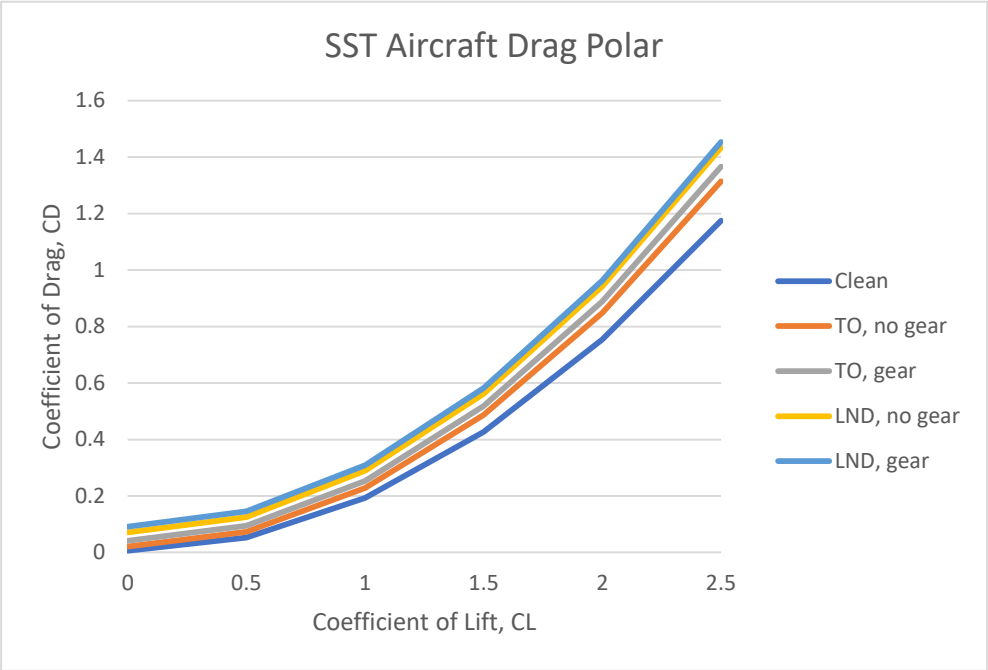

Discussion

This drag polar presents the following max L/D ratios at the different flight conditions. These values allow preliminary analysis of whether the aircraft being designed will be able to meet the required L/D for the cruise condition. Based on these L/D values, this aircraft seems to be well on its way to meeting the high speed, clean L/D.

Table 10. *Maximum L/D Values Found from Drag Polar*

Condition	L/D
Clean, low speed	9.5
TO, no gear	6.9
TO, gear	5.3
LND, no gear	4
LND, gear	3.4

Conclusions

Recent events have seen the emergence of more small supersonic business jets in an effort to reawaken supersonic flight. It was widely known that the Concorde failed due to being uneconomical, breaking even on operational costs on full flights. It is shown in this report that cruising faster (Mach 3), with 150 passengers and a larger range of 4534 n. mi is not only possible but has the potential to be more economical than the Concorde. These design parameters came in at weight that is about 50,000 lbs less than that of the Concorde, which

is a major factor in the operational costs of an aircraft. This design also presents parameters that are essential in reducing the sonic boom. The highly swept wings ensure that the Mach cone formed from the nose of the aircraft is at the leading edge of the wing so that a second shock wave cannot occur. This second shock wave would increase drag, lowering the cruise efficiency of the aircraft. Use of the V-Tail reduces the number of control surfaces and therefore reduces drag and increases the cruise efficiency of the aircraft.

While the next low boom, supersonic flight is expected to take place in the next few years, this is a unique proposal in that it presents a full-sized transport capable of carrying more passengers than any current proposals.

References

A-12 Utility Flight Manual. (1965). *Central Intelligence Agency*, 1.

Boom Technology SST (XB-1) Supersonic Transport Passenger Airliner - United States. (2019). Retrieved February 24, 2019, from https://www.militaryfactory.com/aircraft/detail.asp?aircraft_id=1662.

Brake, A. (2016). NASA designs supersonic passenger jet for overland flights. Retrieved February 24, 2019, from https://www.dezeen.com/2016/03/03/nasa-quiet-supersonic-passenger-jet-overland-flights-plane-aircraft-design-lockheed-martin/.

Ciornei. (2005). Mach number, relative thickness, sweep and lift coefficient of the wing - An Empirical Investigation of Parameters and Equations. *Department of Automotive and Aeronautical Engineering*.

CONCORDE SST. (2003). Retrieved February 24, 2019, from http://www.concordesst.com/.

Francillon, R. J. (1988). McDonnell Douglas Aircraft Since 1920. *Naval Institute Press*, *1*.

Frawley, G. (2000). Boeing X-32 JSF Combat Aircraft since 1945. *London Aerospace Publications*.

Hammond, S. (2017). The Business Case for Supersonic Overland. Retrieved February 24, 2019, from https://niskanencenter.org/blog/supersonic-overland/

Li, W., & Rallabhandi, S. (2014). Inverse Design of Low-Boom Supersonic Concepts Using Reversed Equivalent-Area Targets. *Journal of Aircraft*, *51*(1), 29–36. https://doi.org/10.2514/1.C031551.

Loftin, L. K. J. (n.d.). SP-468: Quest for Performance - The Evolution of Modern Aircraft. *NASA*.

Lugg, R. (2013). *US20150108269A1*. United States. Retrieved from https://patents.google.com/patent/US20150108269A1/en.

Lyu, Z., & Martins, J. R. R. A. (2014). Aerodynamic Design Optimization Studies of a Blended-Wing-Body Aircraft. *Journal of Aircraft*, *51*(5), 1604–1617. https://doi.org/10.2514/1.C032491.

Mercer, C. E., & Carson, G. T. . J. (1979). Transonic aerodynamic characteristics of a supersonic cruise aircraft research model with the engines suspended above the wing. Retrieved from https://ntrs.nasa.gov/search.jsp?R=19800004742&hterms=supersonic+aircraft+wing&qs=N%3D0%26Ntk%3DAll%26Ntt%3Dsupersonic%2520aircraft%2520wing%26Ntx%3Dmode%2520matchallpartial.

Miller, J. (2001). *The X-planes : X-1 to X-45*. Midland Pub. Retrieved from https://bo

oks.google.com/books/about/The_X_planes.html?id=qPpTAAAAMAAJ.
Pace, S. (2004). Lockheed SR-71 Blackbird. *Crowood Press*.
Raymer. (2012). *Aircraft Design: A Conceptual Approach*. AIAA Education.
Roskam, J. (1997). *Airplane Design: Preliminary Configuration Design and Integration of the Propulsion System*. DARCorporation.
Roskam, J. (2000). *Airplane Design: Preliminary Calculation of Aerodynamic, Thrust, and Power Characteristics*. DARCorporation.
Roskam, J. (2002). *Airplane Design: Layout Design of Cockpit, Fuselage, Wing and Empennage*. DARCorporation.
Roskam, J. (2003). *Airplane Design: Preliminary sizing of airplanes*. DARCorporation.
Sun, Y., & Smith, H. (2017). Review and prospect of supersonic business jet design. *Progress in Aerospace Sciences*, *90*, 12–38. https://doi.org/10.1016/J.PAEROSCI.2016.12.003.
Trefny, C. J., Hirt, S. M., Anderson, B. H., Fink, L. E., & Magee, T. E. (2014). Performance of a Supersonic Over-Wing Inlet with Application to a Low-Sonic-Boom Aircraft. Retrieved from https://ntrs.nasa.gov/search.jsp?R=20140011175&hterms=supersonic+aircraft+wing&qs=N%3D0%26Ntk%3DAll%26Ntt%3Dsupersonic%2520aircraft%2520wing%26Ntx%3Dmode%2520matchallpartial.
TU-144 SST. (2003). Retrieved February 24, 2019, from http://www.tu144sst.com/index.html.
Walter, F., Morgenstern, J., Lee, H., Quayle, B., Hajic, K., Scarcello, J., & Arslan, A. (2003). *US006824092B1*. United States. Retrieved from https://patents.google.com/patent/US6824092B1/en.
Wood, & M., R. (1988). Supersonic aerodynamics of delta wings. Retrieved from https://ntrs.nasa.gov/search.jsp?R=19880008231&hterms=supersonic+wings&qs=N%3D0%26Ntk%3DAll%26Ntt%3Dsupersonic%2520wings%26Ntx%3Dmode%2520matchall.
Wood, R. M., Byrd, J. E., & Wesselmann, G. F. (1992). Influence of airfoil geometry on delta wing leading-edge vortices and vortex-induced aerodynamics at supersonic speeds. Retrieved from https://ntrs.nasa.gov/search.jsp?R=19920010796&hterms=supersonic+wings&qs=N%3D0%26Ntk%3DAll%26Ntt%3Dsupersonic%2520wings%26Ntx%3Dmode%2520matchall.